PONTIFICIA UNIVERSIDAD CATÓLICA DE CHILE
ESCUELA DE INGENIERÍA

MULTISCALE MODELING OF CARDIAC ELECTROPHYSIOLOGY: A NON-LINEAR DIFFUSION APPROACH TO THE ELECTRICAL EXCITATION OF CARDIAC TISSUE

SEBASTIÁN ANDRÉS CASTRO HERNÁNDEZ

Thesis submitted to the Office of Research and Graduate Studies
in partial fulfillment of the requirements for the degree of
Master of Science in Engineering

Advisor:
DANIEL ESTEBAN HURTADO SEPÚLVEDA

Santiago de Chile, January 2015

© MMXV, SEBASTIÁN ANDRÉS CASTRO HERNÁNDEZ

PONTIFICIA UNIVERSIDAD CATÓLICA DE CHILE
ESCUELA DE INGENIERÍA

MULTISCALE MODELING OF CARDIAC ELECTROPHYSIOLOGY: A NON-LINEAR DIFFUSION APPROACH TO THE ELECTRICAL EXCITATION OF CARDIAC TISSUE

SEBASTIÁN ANDRÉS CASTRO HERNÁNDEZ

Members of the Committee:
DANIEL ESTEBAN HURTADO SEPÚLVEDA
PABLO IRARRÁZAVAL MENA
ALESSIO GIZZI
DIEGO JAVIER CELENTANO

Thesis submitted to the Office of Research and Graduate Studies
in partial fulfillment of the requirements for the degree of
Master of Science in Engineering

Santiago de Chile, January 2015

© MMXV, SEBASTIÁN ANDRÉS CASTRO HERNÁNDEZ

To my parents, Gerardo Castro and María Elena Hernández, for their complete support all this time.

ACKNOWLEDGEMENTS

I wish to thank to my advisor, Professor Daniel Hurtado Sepúlveda for his guidance, support and help during this work. I am thankful for the time he spent advising and helping me to conduct this thesis. I also want to thank to professors Alessio Gizzi, Diego Celentano, Pablo Irarrázaval and Amador Guzmán for their comments and advices during the thesis development.

I also want to thank to my friends Alan Poulos, Felipe Arróspide, Felipe Pastén, Cristóbal Valderrama, Ernesto Ortiz, José Pinto, Antonio Salazar, Felipe Toro, Mathias Gelb, María de los Ángeles Jordán, Daniel González, Felipe Sanz, Gaspar Auad, Diego Pizarro, Antonio Martinez and Claudia Álvarez, who gave me a pleasent place to work and provided me support and advice.

I also thank to the Chilean Fondo Nacional de Ciencia y Tecnología (FONDECYT) for their support through grant # 11121224, and to the Biomedical Imaging Center at PUC for providing magnetic-resonance images of a human heart.

Finally, I thank to my parents, siblings, and all my family for stay always with me during this process. I am very thankful of their support.

TABLE OF CONTENTS

LIST OF FIGURES

LIST OF TABLES

ABSTRACT

The electrophysiological behavior of excitable biological media has been traditionally modeled using the cable equation. To account for the propagating nature of electrical waves, virtually all cardiac electrophysiology formulations proposed to date consider a linear diffusion flux motivated by ohmic materials, a constitutive relation known in biology as Fick's law. In this work, inspired by the porous nature of gap junctions at intercalated discs in cardiomyocytes that mediate intercellular flux, we propose a novel formulation of cardiac electrophysiology that incorporates a nonlinear diffusion term of the porous-media kind. The resulting system of non-linear partial differential equations are solved using a non-linear implicit finite-element scheme that is suitable for simulations of large-scale cardiac domains. We show that the proposed porous-medium electrophysiology model results in propagating action potentials that have well-defined wavefronts. We also show that the proposed model captures the restitution properties of cardiac tissue in similar way as the cable model does. We demonstrate the capabilities of our method by simulating the activation sequence of a three-dimensional human biventricular heart geometry, where important microstructural features like cardiomyocyte fiber orientation and the His-Purkinje activation network can be succesfully incorporated into the simulation.

Keywords: cardiac electrophysiology, nonlinear diffusion, porous medium equation, His-Purkinje network.

RESUMEN

El comportamiento electrofisiológico de componentes biológicas ha sido, tradicionalmente, modelado utilizando el modelo de cable. Para representar la naturaleza de las ondas eléctricas, practicamente todas las formulaciones electrofisiológicas propuestas a la fecha consideran una difusión lineal del flujo basada en materiales óhmicos, conocida en biología como la ley de Fick. En este trabajo, inspirados por la naturaleza porosa de las uniones gap ubicadas en los discos intercalados de los cardiomiocitos, los cuales controlan el flujo intercelular, proponemos una nueva formulación de electrofisiología cardiaca que incorpora un término de difusión no lineal del tipo medio-poroso. El sistema resultante de ecuaciones diferenciales parciales no lineales es resuelto utilizando un método implícito con elementos finitos, el cual es adecuado para simulaciones a gran escala. Los resultados obtenidos con la utilización del modelo de medio poroso muestran potenciales de acción con frentes de onda bien definidos y que viajan con una velocidad finita. También se muestra que este modelo captura las características de restitución de un músculo cardiaco de igual manera que la ecuación de cable lo hace. Finalmente mostramos las capacidades de nuestro método simulando la secuencia de activación en un modelo tridimensional del corazón humano, donde importantes microestructuras fueron incorporadas, como la orientación de los cardiomiocitos, el haz de His y la red de Purkinje.

Palabras claves: electrofisiología cardiaca, difusión no-lineal, ecuación de medio poroso, red de Purkinje.

1. INTRODUCTION

1.1. Motivation

Since the last six decades, the interaction between mathematics and biology has grown considerably. The number of physiological functions that can be described in mathematical terms is summarized by Keener and Sneyd (2008a): physiology is the biological science where mathematics has played the greatest role.

However, in order to model the physiology of systems, it is necessary to recognize that every system is composed by different levels working together, from microscopic to macroscopic scales, and that every scale has to be modeled in an accurate way. These complex phenomena are usually classified as chemical, electrical or mechanical effects, and are studied in the different organs of the human body. For the chemical scale some options are the Hodgkin-Huxley model (Hodgkin & Huxley, 1952), the ten Tusscher model (ten Tusscher, Noble, Noble, & Panfilov, 2004) or the Aliev-Panfilov model (Aliev & Panfilov, 1996). For the electrical part the options are the cable model (Hodgkin & Huxley, 1952) or the bidomain and monodomain model (Tung, 1978), and for the mechanical behavior several models of the elasticity of the myocardium are available, including isotropic models (Demiray, 1976), transversely isotropic models (Guccione, McCulloch, & Waldman, 1991; Costa et al., 1996) and orthotropic models (Schmid, Nash, Young, & Hunter, 2006; Holzapfel & Ogden, 2009). A complete review of mathematical models in cardiology can be found in Schmid and Hunter (2009).

In this work, we propose a computational approach to study the electrical behavior of the heart. In particular, we focus on the sole electrical and chemical behaviors, where several mathematical models have attemped to reproduce the complex behavior of both cardiac cells and tissue.

Although these models have successfully reproduced many of the features of the electrical behavior of cardiac cells, complex behaviors such as alternans and arrhythmias necessitate further advances from the mathematical point of view. This introduces the possibility to use a generalization of the standard model of the electrical flux as seen in the porous medium equation (Vasquez, 2006).

1.2. Cardiac electrophysiology

The heart is located in the centre of the chest cavity between the right and left lungs, and it consists of four chambers: the right and left ventricle, and the right and left atrium. In Figure 1.1 these chambers are shown in detail. The heart's pumping function depends on the contraction and relaxation of the atria and ventricles.

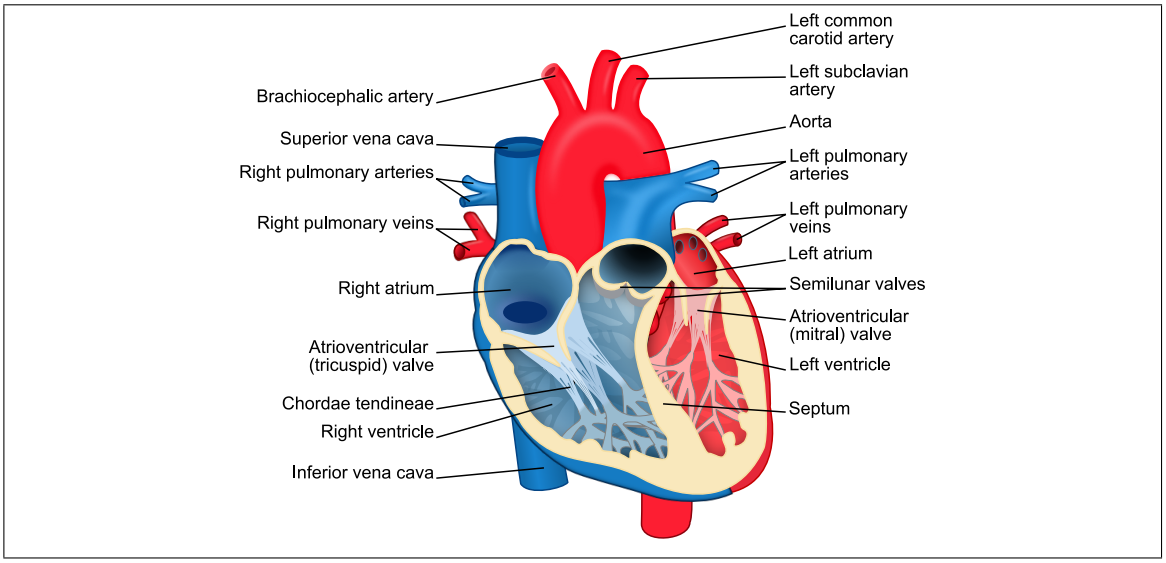

Figure 1.1. Heart anatomy

The cardiac cycle is coordinated by a series of electrical impulses that start from the sinoatrial node, located in the right atrium of the heart. This impulspe propagates through the atrial wall, generating a coordinated contraction that ejects the blood from the atria to the ventricles. The electrical pulse reaches the atrioventricular node, between the right atrium and the right ventricle. From this node, the electrical impulse enters to the Bundle

of His and the Purkinje fibers, where it is propagated through the ventricular myocardium, producing the contraction of the right and left ventricles. The blood in the right ventricle is pumped up through the pulmonary valve and the pulmonary artery to the lungs, while the left ventricle pumps oxygenated blood to tissues all over the body. These phases are called atrial and ventricular systole, respectively. When the heart starts to relax, first the ventricular muscles and then the atrium muscles, the phase is named diastole. Finally, this process is repeated about 80 times per minute in a healthy subject under resting conditions, although it varies according to the physiological conditions.

The electrical activity of the heart is analyzed at different scales. First the cellular scale, where the behavior of individual myocytes is studied, and later the tissue scale, at which the interaction between all the cells in the muscle is observed.

1.2.1. Cellular scale

Similarly to all electrically active cells in the human body, cardiac cells are characterized by a membrane potential (action potential) that governs their electrical activity. In particular, it is a balance between the electrical and chemical gradients across the cell membrane. While the electrical gradient, or capacitive current, is generated by the movements of electrons relative the membrane surface, chemicals gradients are associated to the ions present in both inside and outside of the cell, and the permeability of the cell membrane. Despite the several different ions present inside and outside the cell, three ions species are more important for the membrane voltage dynamics, i.e.: Na^+, K^+ and Ca^{++}. The flux of such ion species across the cell membrane is typically known as ionic currents.

The ionic currents are responsible for the onset, development and return to resting state of an action potential in the cell. An inward current, according to electrophysiological convention (Katz, 2006), is the flux of charge that would occur if a positive ion moved across the membrane into the cell, while an outward current occur when a positively charged ion leaves the cell interior. The inward and outward currents can be generated by the opposite movement of negative ions, i.e. when a negative ion leaves the cell it corresponds to an

inward current and when a negative ion enters to the cell is a outward current. Table 1.1 shows a detailed description of the three principal ion currents cited.

Action potentials are normally initiated by capacitive currents that are generated when a depolarization wave approaches to a resting cell. When the membrane depolarizes, the voltage-gated ion channels open and allow for the inward and outward current movement.

Table 1.1. Principal ion currents for an action potential. Values of concentration from Klabunde (2005)

Ion	Charge	Inside Concentration	Outside Concentration	Current Generated	Effect on Membrane Potential
Calcium	Positive	0.0001 mM	2.5 mM	Inward	Depolarization
Sodium	Positive	20 mM	145 mM	Inward	Depolarization
Potasium	Positive	150 mM	4 mM	Outward	Repolarization

After this rapid depolarization, an initial repolarization occurs caused by the potassium channels and the inactivation of the sodium channels. However, the calcium inward current is slower than the sodium one and the repolarization is delayed until the channels of calcium are blocked and the cell returns to the resting potential. This interaction can be seen in Figure 1.2.

The flow of current across the cell membrane is usually modeled as an electric circuit, see in Figure 1.3. Considering that the different ion channels work in parallel, the total ionic current is the sumation over all the contributions, i.e.

$$I_{ion} = \sum_{x} I_x. \tag{1.1}$$

The action potential inside (ϕ_i) and outside of the cell (ϕ_e), the ionic currents (I_{ion}) and the capacitive current (I_s) are related according to the Equation (1.2)

$$\frac{\mathrm{d}V_m}{\mathrm{d}t} = -\frac{(I_{ion} + I_s)}{C_m} \tag{1.2}$$

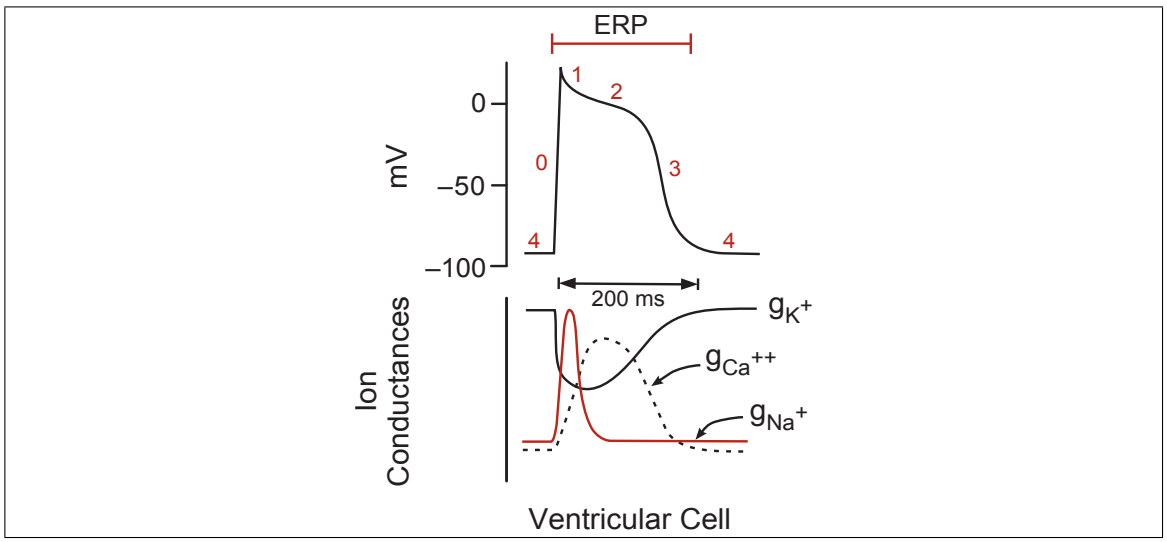

Figure 1.2. Changes in ion conductances associated with a ventricular myocite action potential. Phase 0 (depolarization) is due to the rapid increase in sodium conductance and the fall in potasium conductance. Phase 1 (initial repolarization) is due to the opening of special potassium channels and the inactivity of the sodium channels. Phase 2 (plateu) is due to the slow inward current of the calcium. Phase 3 (repolarization) results from the decrease of calcium and increase of potasium. Phase 4 (resting potential) occurs when channels and concentrations returns to their initial conditions. Figure extracted from Klabunde (2005)

where C_m is the capacitance and the transmembrane potential is defined as

$$V_m = \phi_i - \phi_e. \tag{1.3}$$

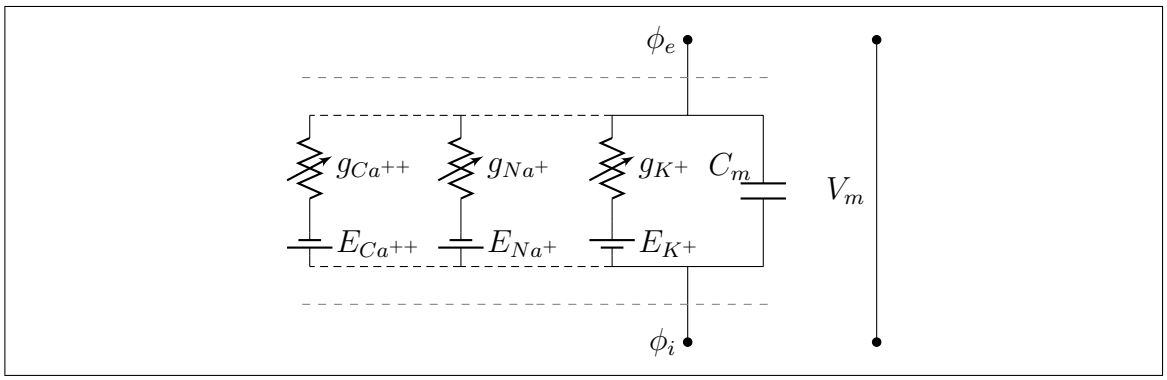

Figure 1.3. Electric circuit analogy to cardiac cell behavior

There are several models that attemp to describe the interaction between the different ionic species across the cell membrane, generally called *biophysical models*. However, these models present a high level of complexity in order to recover a realistic response of the action potential. For thit reason, simplified models have been proposed, known as *phenomenological models*. These type of models are simpler and more efficient in a computational perspective, although they do not recover all the nonlinear dynamics characteristic of the cardiac action potential. In the following sections, some models of both types are briefly described.

1.2.1.1. Biophysical models

- Hodgkin and Huxley model

  One of the most important works in the field of electrophysiology is the model presented by Hodgkin and Huxley (1952). That work has been the basis of virtually all biophysical models of cardiac cells. This model separates the ionic current into three components: current carried by sodium ions (I_{Na}), current carried by potasium ions (I_K) and a leakage current that represent other ions (I_L). In this case, Equation (1.1) is expresed as

$$I_{ion} = I_{Na} + I_K + I_L \tag{1.4}$$

  where

$$I_{Na} = \bar{g}_{Na} m^3 h \left(V_m - E_{Na}\right) , \tag{1.5}$$

$$I_K = \bar{g}_K n^4 \left(V_m - E_K\right) , \tag{1.6}$$

$$I_L = \bar{g}_L \left(V_m - E_L\right) . \tag{1.7}$$

The variables h, m and n are dimensionless gating variables controlled by

$$\frac{\mathrm{d}h}{\mathrm{d}t} = 0.07 \exp\left[\frac{V_m}{20}\right](1-h) - \frac{h}{\exp\left[0.1\,(V_m+30)\right]+1} \tag{1.8}$$

$$\frac{\mathrm{d}m}{\mathrm{d}t} = \left(\frac{0.1\,(V_m+25)}{\exp\left[0.1\,(V_m+25)\right]-1}\right)(1-m) - 4\exp\left[\frac{V_m}{18}\right]m \tag{1.9}$$

$$\frac{\mathrm{d}n}{\mathrm{d}t} = \left(\frac{0.02\,(V_m+10)}{\exp\left[0.1\,(V_m+10)\right]-1}\right)(1-n) - 0.125\exp\left[\frac{V_m}{80}\right]n \tag{1.10}$$

- Ten Tusscher model

  The ten Tusscher model (ten Tusscher et al., 2004) is one of the most accurate biophysical description of the cardiac action potential. In this model, the total ionic current is the sum of the following contributions

$$\begin{aligned} I_{ion} = I_{Na} + I_{K1} + I_{to} + I_{Kr} + I_{Ks} + I_{CaL} + I_{NaCa} \\ + I_{NaK} + I_{pCa} + I_{pK} + I_{bCa} + I_{bNa} \end{aligned} \tag{1.11}$$

  where I_{NaCa} is Na^+/Ca^{2+} exchanger current, I_{NaK} is Na^+/K^+ pump current, I_{pCa}, I_{pK} are plateu Ca^{2+} and K^+ currents, and finally I_{Kr} and I_{Ks} are the rapid and slow delayed rectifier current. The other currents are referred to the original paper. This model has a total of 17 variables.

Though these models allow to explain some differences between endocardial and epicardial cells, they require a considerable level of computational power, making them difficult to use for large scale simulations. For this reason, phenomenological models arise as a reliable option if a macroscopic analysis is required instead of a very detailed description of the ion channels.

1.2.1.2. Phenomenological models

- FitzHugh-Nagumo model

  The FitzHugh-Nagumo model (FitzHugh, 1961; Nagumo, Arimoto, & Yoshizawa, 1962) is a polynomial model with a recovery variable. This model represents one of the most adopted mathematical description for excitable cells. The ionic

current is given by

$$I_{ion} = -C_m \left(V_m - V_r\right) \frac{\mathrm{d}u}{\mathrm{d}t} \tag{1.12}$$

with the nondimensional membrane potential given by

$$u = \frac{V_m - V_r}{V_p - Vr}$$

and

$$\frac{\mathrm{d}u}{\mathrm{d}t} = c_1 u \left(u - \alpha\right)\left(u - 1\right) + c_2 \nu \,, \tag{1.13}$$

$$\frac{\mathrm{d}\nu}{\mathrm{d}t} = b \left(u - d\nu\right). \tag{1.14}$$

The parameters V_r and V_p are used to indicate the resting and plateu potential, while α indicates the threshold where the cell activates.

- Aliev-Panfilov model

  Following the FitzHugh-Nagumo model as a basis, Aliev and Panfilov (1996) proposed a modification of the recovery variable ν. In Equation (1.13) and for the recovery variable in Equation (1.14) they proposed to use the following expressions:

$$\frac{\mathrm{d}u}{\mathrm{d}t} = c_1 u \left(u - \alpha\right)\left(u - 1\right) + c_2 u \nu \,, \tag{1.15}$$

$$\frac{\mathrm{d}\nu}{\mathrm{d}t} = \left[\gamma + \frac{\mu_1}{\mu_2 + u}\nu\right]\left[-\nu - c_1 u \left(u - b - 1\right)\right] \tag{1.16}$$

- Minimal model

  The minimal model (Bueno-Orovio, Cherry, & Fenton, 2008) is able to recover the general behavior of inward and outward currents, defining three currents: fast inward (I_{fi}), slow outward (I_{so}) and slow inward (I_{si}):

$$I_{fi} = -v\mathcal{H}\left(u - \theta_v\right)\left(u - \theta_v\right)\left(u_u - u\right)/\tau_{fi} \tag{1.17}$$

$$I_{so} = \left(u - u_o\right)\left(1 - \mathcal{H}\left(u - \theta_w\right)\right)/\tau_o + \mathcal{H}\left(u - \theta_w\right)/\tau_{so} \tag{1.18}$$

$$I_{si} = -\mathcal{H}\left(u - \theta_w\right) ws/\tau_{si} \tag{1.19}$$

where $\mathcal{H}$ is the Heaviside step function. The differential equations for v, w and s are

$$\frac{\mathrm{d}v}{\mathrm{d}t} = \left(1 - \mathcal{H}\left(u - \theta_v\right)\right)\left(v_\infty - v\right)/\tau_v^- - \mathcal{H}\left(u - \theta_v\right)v/\tau_v^+ \tag{1.20}$$

$$\frac{\mathrm{d}w}{\mathrm{d}t} = \left(1 - \mathcal{H}\left(u - \theta_w\right)\right)\left(w_\infty - w\right)/\tau_w^- - \mathcal{H}\left(u - \theta_w\right)w/\tau_w^+ \tag{1.21}$$

$$\frac{\mathrm{d}s}{\mathrm{d}t} = \left(\left(1 + \tanh\left(k_s\left(u - u_s\right)\right)\right)/2 - s\right)/\tau_s \tag{1.22}$$

This model is called Minimal because it requires only three additional variables to recover a realistic shape of the action potential, similar that obtained with physiological models.

Many other electrophysiology models, biophysical and phenomenological, haven been proposed in the literature. For more information, Pullan, Cheng, and Buist (2005) and Fenton and Cherry (2008) present a large review of different cardiac cell models.

1.2.2. Tissue scale

In this section we describe the interaction between the different cells in the myocardium. From this point there is a spatial component associated to the location of the cell in the heart. To understand its interaction, it is necessary to see how cells are distributed in the organ structure. Figure 1.4 shows how cardiac cells are connected by gap junctions arranged within sheets containing collagen and extracellular fluids.

The orientation of the cardiac cells gives the first microstructural axis called the *fibre axis*. These fibres lie on a network of sheets, where it is possible to define a second direction called *sheet axis*. Finally, a third direction is defined as the cross product between the fibre axis and the sheet axis, known as the *cross-sheet axis*.

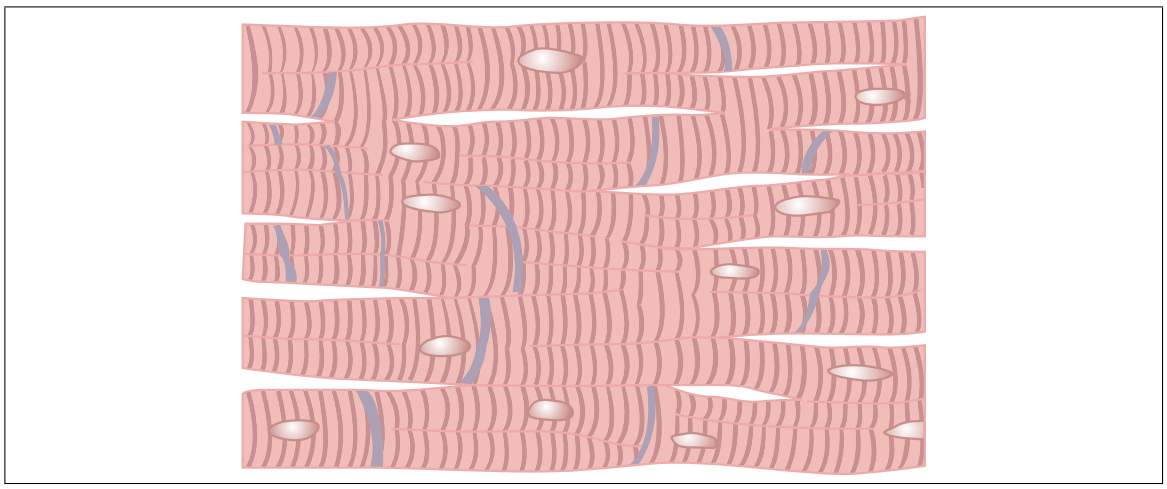

Figure 1.4. Cardiac cell coupling. Figure extracted from Guyton and Hall (2006)

1.2.2.1. Cable model

To describe the propagation of an action potential along the length of a muscle fibre in a continuum framework, the electrical circuit in Figure 1.5 is usually adopted. Cardiac cells are modeled as described in Section 1.2.1 with an equivalent resistance R_m and a capacitance C_m. The intracellular and extracellular space are modeled using resistances in series R_i and R_e respectively.

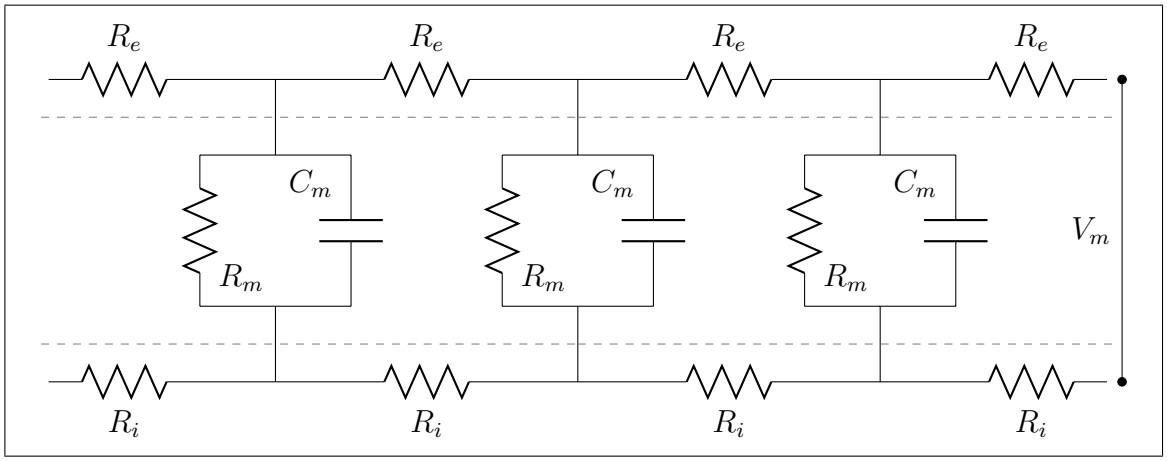

Figure 1.5. Circuit representation of the cable model

Considering a length of fibre l with an intracellular cross sectional area A_i and an extracellular cross sectional A_e, we can define the resistivities by

$$r_i = \frac{R_i A_i}{l} \qquad \text{and} \qquad r_e = \frac{R_e A_e}{l}. \tag{1.23}$$

Using the Ohm's law, the change in the intracellular field ϕ_i over a small length along the fibre Δx is given by

$$\frac{\Delta \phi_i}{\Delta x} = -I_i r_i \xRightarrow[\Delta x \to 0]{} \frac{\mathrm{d}\phi_i}{\mathrm{d}x} = -I_i r_i \tag{1.24}$$

and similarly for the extracellular potential ϕ_e

$$\frac{\mathrm{d}\phi_e}{\mathrm{d}x} = -I_e r_e. \tag{1.25}$$

Aplying now the Kirchhoff's first law in the intra and extracellular spaces we have

$$I_i = (I_i + \Delta I_i) + I_m \Delta x \Longrightarrow \frac{\partial I_i}{\partial x} = -I_m \tag{1.26}$$

$$I_e = (I_e + \Delta I_e) - I_m \Delta x \Longrightarrow \frac{\partial I_e}{\partial x} = I_m \tag{1.27}$$

where I_m is the transmembrane current per unit length. Using the definition in Equation (1.3) and performing the balance of currents across the cell membrane, we get

$$\begin{aligned} \frac{\partial^2 V_m}{\partial x^2} &= \frac{\partial^2 \phi_i}{\partial x^2} - \frac{\partial^2 \phi_e}{\partial x^2} \\ &= \frac{\partial}{\partial x}\left(-I_i r_i + I_e r_e\right) \\ &= I_m \left(r_i + r_e\right) \end{aligned} \tag{1.28}$$

For the circuits that represent the cardiac cells, the total current I is equal to the sum of each current, i.e.

$$I = \frac{V_m}{R_m} + C_m \frac{\partial V_m}{\partial t}. \tag{1.29}$$

This can be expressed as a current per unit volume by multiplying by the surface area for a given length of fibre and dividing by the volumen enclosed by this surface (Pullan et al., 2005), denoted as A_m. In addition, V_m/R_m is the sum of the ionic currents described before, i.e. I_{ion}, so Equation (1.29) yields

$$I_m = A_m \left(I_{ion} + C_m \frac{\partial V_m}{\partial t} \right) \tag{1.30}$$

Replacing Equation (1.30) in Equation (1.28), the cable model is given by

$$\frac{1}{r_i + r_e} \frac{\partial^2 V_m}{\partial x^2} = A_m \left(C_m \frac{\partial V_m}{\partial t} + I_{ion} \right) \tag{1.31}$$

or, in terms of the intra and extracellular conductance σ_i and σ_e, the final form of the active cable equation is

$$\frac{\sigma_i \sigma_e}{\sigma_i + \sigma_e} \frac{\partial^2 V_m}{\partial x^2} = A_m \left(C_m \frac{\partial V_m}{\partial t} + I_{ion} \right). \tag{1.32}$$

1.2.2.2. Bidomain model

To extend the cable theory to a more physical interaction between intracellular and extracellular spaces, the bidomain model, first formulated by Tung (1978), is usually adopted. The bidomain model considers an intracellular and extracellular domains that occupy the same physical space according to the classical homogeneization theories. By using Ohm's law, the current density vector $\boldsymbol{J}$ is defined as

$$\boldsymbol{J} = \boldsymbol{\sigma} \boldsymbol{E} \tag{1.33}$$

where $\boldsymbol{\sigma}$ is the conductivity tensor and $\boldsymbol{E}$ is the electric field vector. Considering a quasi-static assumption, and the corresponding Maxwell-Faraday equation, it is possible to define the electric field as the gradient of a scalar potential field, i.e. $\boldsymbol{E} = -\nabla \phi$, so the intra and extracellular current density are defined as

$$\boldsymbol{J}_i = -\boldsymbol{\sigma}_i \nabla \phi_i \tag{1.34}$$

$$\boldsymbol{J}_e = -\boldsymbol{\sigma}_e \nabla \phi_e. \tag{1.35}$$

Any current that leaves one of the two domains must cross the cell membrane and flow into the other domain. Therefore, the change in current density in each domain must be equal in magnitude and opposite sign, and also equal to the flow across the cell membrane.

$$-\nabla \cdot \boldsymbol{J}_i = \nabla \cdot \boldsymbol{J}_e = A_m I_m \tag{1.36}$$

where A_m is the surface to volume ratio and I_m is the transmembrane current density per unit area.

Substituting (1.34) and (1.35) in (1.36), a system of two coupled equations is generated

$$\nabla \cdot (\boldsymbol{\sigma}_i \nabla \phi_i) = A_m I_m \tag{1.37}$$

$$\nabla \cdot (\boldsymbol{\sigma}_e \nabla \phi_e) = -A_m I_m \,. \tag{1.38}$$

In addition, the transmembrane current density per unit area can be written as

$$I_m = C_m \frac{\partial V_m}{\partial t} + I_{ion} \,. \tag{1.39}$$

So to combine the Equations (1.37) and (1.38) with (1.39). The detailed derivation of the bidomain equations can be found in several books (Pullan et al., 2005; Keener & Sneyd, 2008b). Here, the classical equations are presented:

$$\nabla \cdot \left(\left(\boldsymbol{\sigma}_i + \boldsymbol{\sigma}_e \right) \nabla \phi_e \right) = -\nabla \cdot \left(\boldsymbol{\sigma}_i \nabla V_m \right) \,, \tag{1.40}$$

$$\nabla \cdot (\boldsymbol{\sigma}_i \nabla V_m) + \nabla \cdot (\boldsymbol{\sigma}_i \nabla \phi_e) = A_m \left(C_m \frac{\partial V_m}{\partial t} + I_{ion} \right) . \tag{1.41}$$

If the domains are assumed to be equally anisotropic ($\boldsymbol{\sigma}_i = k\boldsymbol{\sigma}_e$), and considering an external stimulus current I_s, the bidomain equations can be simplified in to the monodomain equation given by

$$\nabla \cdot (\boldsymbol{\sigma} \nabla V_m) = A_m \left(C_m \frac{\partial V_m}{\partial t} + I_{ion} \right) - I_s \tag{1.42}$$

where we recover the single field V_m described by the cable model.

1.3. Porous medium equation

The porous medium equation,

$$\frac{\partial u}{\partial t} = \frac{1}{m+1}\Delta_x \left(u^{m+1}\right) \, , \, m > 0 \, , \tag{1.43}$$

is one of the simplest examples of nonlinear evolution equation of parabolic type (Vasquez, 2006). Here, $u = u(\boldsymbol{x}, t)$ is a nonnegative scalar function of space and time. It is clear to see that for $m = 0$ we recover the classical heat equation, its most famous relative.

Applying the porous medium formulation to cardiac electrophysiology model, we can write Equation (1.43) in its complete version as

$$\frac{\partial u}{\partial t} = \operatorname{div} \left(\boldsymbol{D}(u)\nabla u\right) + f(u) \tag{1.44}$$

where $\boldsymbol{D}(u)$ is the diffusion coefficient. In this case we have that

$$\boldsymbol{D}(u) = \boldsymbol{D}u^m. \tag{1.45}$$

Expanding the divergence term we obtain

$$\frac{\partial u}{\partial t} = m\boldsymbol{D}u^{m-1}||\nabla u||^2 + \boldsymbol{D}u^m\Delta u + f(u) \tag{1.46}$$

it is possible to note that for $u \neq 0$ the right side of the equation is controlled by the term $\boldsymbol{D}u^m\Delta u$, but for $u \to 0$ the equation simplifies to $\partial_t u \sim m\boldsymbol{D}u^{m-1}||\nabla u||^2$, a modified *eikonal equation*.

The principal characteristic that can be found in the porous medium equation is the property called *finite propagation*. This property is in strong contrast to the *infinite propagation* obtained in the heat equation. A simple explanation is given by Vasquez (2006):

- Heat Equation: *A non-negative solution of the heat equation is automatically positive everywhere in its domain of definition*, and

- Porous Medium Equation: *Disturbances from the level* $u = 0$ *propagate in time with finite speed for solutions of the porous medium equation.*

The finite propagation can be seen as a free boundary, or interface, that separates regions where the solution is positive from the regions where $u = 0$. It is clear that this property supports the physical soundness of the porous medium equation to model diffusion as the electrical wave in the cardiac tissue.

1.4. Thesis structure

This document is divided into four chapters, which are briefly explained below.

In Chapter 1, the motivation and the theorical framework are presented. The main concepts of cardiac electrophysiology and the porous medium equation are explained, and their governing equations are formulated.

Chapter 2 consists of the article written based on this research, being the principal section of the thesis. The article is composed by an introduction, then the mathematical formulation of the porous medium equation and the geometrical characteristics. Finally, the results of some simulations are shown and an analysis is done.

In Chapter 3 the conclusions are presented with some ideas in Chapter 4 of possible future work in relation with the article.

2. POROUS MEDIUM: A NON-LINEAR DIFFUSION APPROACH TO THE ELECTRICAL EXCITATION OF CARDIAC TISSUE

2.1. Introduction

Excitable biological tissues features a strong microstructural complexity, resulting in a highly heterogeneous and anisotropic behavior both at the macroscopic and microscopic scales (Khaled & Vafai, 2003). However, the phenomenological and biophysical electrophysiology models proposed to date for the dynamic characterization of excitable media are typically formulated in terms of averaged, or homogenized properties of continuum media (Pullan et al., 2005). Upon these assumptions, single-cell models have been extended to the tissue level by incorporating spatial flux terms, to reflect the propagating nature of electrical waves.

In the cardiac electrophysiology field, the last two decades have been characterized by a fast-paced growth of sophisticated mathematical models that can accurately reproduce several electrophysiological features observed in isolated cardiomyocytes, both in healthy and pathological conditions (Clayton et al., 2011). Remarkable advances have been also conducted at the tissue level by means of phenomenological models able to reproduce several spatio-temporal experimental observations (Fenton & Karma, 1998; Bueno-Orovio et al., 2008). However, the complete characterization and understanding of complex phenomena in the cardiac electrical activity, e.g. cardiac alternans and arrhythmias (Watanabe, Fenton, Evans, Hastings, & Karma, 2001; Cherry & Fenton, 2004; Gizzi et al., 2013), remains an open avenue of research, and poses many challenges both at the experimental and theoretical level. Cardiac muscle, as a highly nonlinear excitable media, allows for the propagation of solitary excitation waves and supports spiral waves during arrhythmic events (Bini, Cherubini, Filippi, Gizzi, & Ricci, 2010; Winfree, 1987, 2001), i.e. tachycardia and fibrillation (Cherry & Fenton, 2008; Davidenko, Pertsov, Salomonz, Baxter, & Jalife, 1992). Action potential wavefront propagation as well as repolarization timing, therefore, assume a key role in the onset and development of arrhythmias (Glukhov,

Egorov, Efimov, & Rosenshtraukh, 2012; Fenton, Gizzi, Cherubini, Pomella, & Filippi, 2013; Hurtado & Kuhl, 2014).

Virtually all mathematical models of excitable media derive from the seminal work of Hodgkin and Huxley (1952) on the squid giant axon and are typically formulated in terms of the cable equations, either in their monodomain (Niebur, 2008) or bidomain (Tung, 1978) version. The resulting set of equations constitute a nonlinear reaction-diffusion system (Turing, 1952) in which spatial propagation of electrical potentials are coupled to evolution equations describing the ion-channel, exchanger and pump gate dynamics. The classical cable theory describes the propagation of electric currents along the cell membrane by assuming the excitable cells as Ohmic cylindrical conductors, characterized by segments with transmembrane nonlinear resistances and capacitances, and axially connected via linear resistances, i.e., the gap junctions (Alberts et al., 2007). The bidomain formulation, specifically developed for reproducing electrical propagation in syncytia, consists in a two- or three-dimensional cable model, still assuming that the average behavior spans over the intracellular and extracellular spaces following a linear Fickian diffusion process (Tung, 1978; Henriquez, 1993).

It is currently well established from histological studies that both the intracellular and extracellular spaces in myocardium constitute a highly heterogeneous and anisotropic medium, mainly composed of blood vessels, collagen, fibroblasts, and fat, among others. On such a basis, the homogenization assumptions (Pavliotis & Stuart, 2008) usually made on the monodomain and bidomain formulations have limitations in reproducing the highly nonlinear dynamics emerging from the ensemble of connected cells. Ionic flux in the longitudinal direction of cardiomyocytes, for example, has long been recognized as a continuous-discontinuous process (Spach et al., 1981; Spach, Heidlage, Dolber, & Barr, 1998), with the cytoplasmic domain having a low resistivity, and the intercalated discs presenting a high resistivity. At a submicron scale, intercalated discs can be considered as a porous membrane, where ions can only pass through gap junctions, which are embedded in the non-conductive sarcolemma. Figure 2.1 shows a representative example of the

irregular distribution of Connexin 43 (gap-junction main protein), as well as the porous structure formed at the intercalated discs. The non-smooth nature of ion conduction at

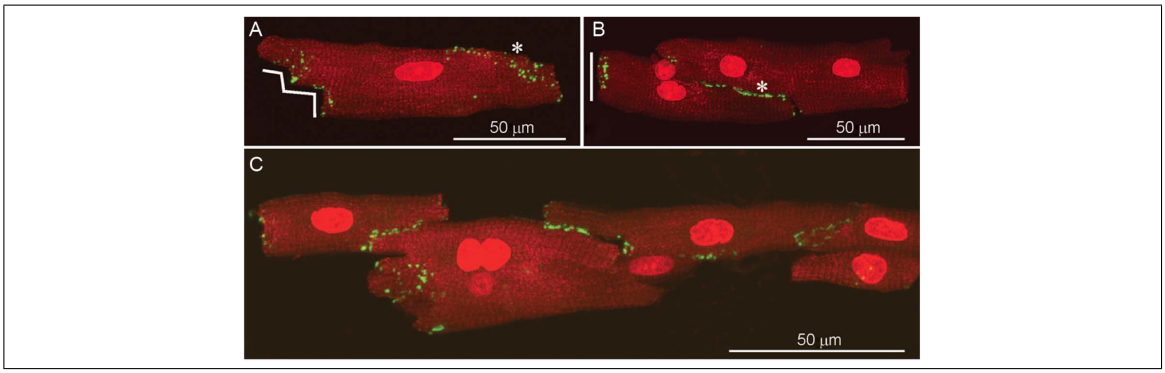

Figure 2.1. Confocal micrograph showing the distribution of gap junctions (Connexin 43, in green) in rat atrial myocytes, predominantly in step-like and straight-end intercalated discs configurations. Reproduced with permission from Severs et al. (2008).

the sub-cellular level is in contrast with the standard linear-diffusion flux employed in the cable theory, for which a natural solution are propagating waves with smooth Gaussian profiles that exhibit an infinite propagation of the information (Friedman, 1964). Such a lack of proper mathematical representation for the spatial propagation of ionic flux calls for novel approaches in the modelling of the intra- and extra-cellular ionic flow in order to take into account the intrinsic tissue multiscale architecture, always focussed on local heterogeneities and applied to realistic scenarios (Fenton et al., 2009; Krishnamurthy et al., 2013; Luther et al., 2011; Nordsletten, Niederer, Nash, Hunter, & Smith, 2011).

Recently, a fractional diffusion formulation has been proposed to model cardiac action potential propagation (Bueno-Orovio, Kay, Grau, Rodriguez, & Burrage, 2014). Non-integer spatial derivatives were introduced in order to reproduce the multiscale effects of transport processes taking place into the heart tissue, with particular interest in the modulation of the total electric field by the secondary electrical sources associated with tissue inhomogeneities. Bueno-Orovio and co-workers showed that structural heterogeneity

modeled by a fractional operator accurately recovers several features of cardiac propagation, as well as naturally incorporating dispersion of repolarization.

The porous medium equation, first proposed by Oleinik, Kalashnikov, and Juj-lin (1958), is a simple and mathematically sound generalization of the heat equation, where the linear diffusion term that results from Fourier's law of heat conduction is replaced by a nonlinear constitutive relation for the heat flux that depends on the magnitude of the field of interest (Vazquez, 1992). Generalizations of the PME have been developed elsewhere (Friedman, 1964; Ladyzhenskaia, Solonnikov, & Ural'ceva, 1968) and successful applications of the PME are found in many areas of the applied sciences and engineering in problems involving fluid flow (Leibenzon, 1930; Muskat & Wyckoff, 1937), heat transfer (Zeldovich & Raizer, 1966) and diffusion (Smoller, 1982). Perhaps one of the most attractive features of the porous medium equation is the fact that the associated solutions are travelling waves that possess a well defined speed of propagation (Vasquez, 2006). Applications of the porous-medium equation in the mathematical biology context, however, are indeed very limited to population dispersal models, i.e. tumor growth (Cherubini, Gizzi, Bertolaso, Tambone, & Filippi, 2012; Murray, 2003), and to the author's knowledge this work constitutes the first use of the porous-medium diffusion in the context of electrical propagation in excitable biological media, such as cardiac tissue. Similarly, very few attempts have been made to describe the behavior of the cardiac tissue as a porous medium from a mechanical point of view (Cookson et al., 2012; Huyghe, Arts, van Campen, & Reneman, 1992).

Drawing ideas from the porous-medium equation, in this work we propose a non-linear diffusion model of cardiac electrophysiology that alleviates some of the theoretical deficiencies of the traditional cable model. To this goal, we propose a modification of the spatial flux term of the cable equation, and study its implications on the electrophysiological response of cardiac tissue by means of numerical simulation of the propagation of action potentials in both simplified 1-D cases, as well as in 3-D media with realistic biventricular geometries.

The manuscript is organized as follows. In Sec. 2.2 we introduce the mathematical formulation of the porous medium model and the numerical scheme adopted. In Sec. 2.2.3 we describe the human heart geometry reconstruction focusing on the algorithms adopted for generating the tissue anisotropy and the specialized activation network. In Sec. 2.3 we compare the numerical simulations between the classical cable theory and the generalized porous-medium formulation of cardiac electrophysiology by considering a simplified phenomenological model for the ventricular wall and the Purkinje network. Discussions and future perspectives are drawn in Sec. 2.4.

2.2. Materials and Methods

2.2.1. Porous-medium model of cardiac electrophysiology

Let $\Omega \in \mathbb{R}^3$ be the cardiac domain where we are interested in modeling the propagation of action potentials during the time interval $[0, T]$, and $V_m : \Omega \times [0, T] \to \mathbb{R}$ the transmembrane potential. Following a monodomain approach, from charge conservation we obtain the governing equation

$$A_m \left(C_m \frac{\partial V_m}{\partial t} + I_{ion}(V_m, \boldsymbol{r}) \right) + \mathrm{div}(\boldsymbol{j}) = 0, \quad (\boldsymbol{x}, t) \in \Omega \times [0, T], \tag{2.1}$$

where A_m, C_m are the surface-to-volume ratio and membrane capacitance, respectively, I_{ion} is the ionic current depending on the transmembrane voltage V_m and a set of state variables $\boldsymbol{r} : \Omega \to \mathbb{R}^{\mathrm{m}}$ which may include gating variables and ion concentrations, and $\boldsymbol{j}$ is the ionic flux spatially propagating through the medium. A common practice is to normalize the transmembrane voltage and rearrange (2.1) to obtain the non-dimensional equation

$$\frac{\partial \phi}{\partial t} + \mathrm{div}(\boldsymbol{q}) - f(\phi, \boldsymbol{r}) = 0, \quad (\boldsymbol{x}, t) \in \Omega \times [0, T], \tag{2.2}$$

where ϕ is the normalized transmembrane potential, $\boldsymbol{q}$ the normalized flux, and $f(\phi, \boldsymbol{r})$ the normalized ionic current.

In addition to equation (2.2), a set of evolution equations for the state variables must be provided, typically of the form

$$\frac{\mathrm{d}\boldsymbol{r}}{\mathrm{d}t} = g(\phi, \boldsymbol{r}), \quad (\boldsymbol{x}, t) \in \Omega \times [0, T]. \tag{2.3}$$

The form of $f(\phi, \boldsymbol{r})$ and $g(\phi, \boldsymbol{r})$ depends on the electrophysiological model chosen to represent the ionic currents of a single cell. The standard assumption in virtually all models based on the monodomain description is the adoption of a constitutive law of the Fick's type, namely

$$\boldsymbol{q} = -\boldsymbol{D}\nabla\phi, \tag{2.4}$$

where $\boldsymbol{D}$ is the normalized conductivity tensor. This assumption leads to the standard cable model of cardiac electrophysiology,

$$\frac{\partial\phi}{\partial t} = \nabla \cdot (\boldsymbol{D}\nabla\phi) + f(\phi, \boldsymbol{r}), \quad (\boldsymbol{x}, t) \in \Omega \times [0, T].$$

In this work, for the reasons explained in the introduction, and other that will be apparent later, we propose a functional relation for the constitutive equation of the kind $\boldsymbol{q} = \boldsymbol{q}(\phi, \nabla\phi)$. In particular, we choose

$$\boldsymbol{q} = -\boldsymbol{D}\phi^m\nabla\phi, \tag{2.5}$$

with $m \in \mathbb{R}^+$. We note here that taking the divergence of (2.5) lead us to the porous-medium diffusion term (Vasquez, 2006). In the sequel, we will refer to (2.2) combined with (2.5), and (2.3) as the *porous-medium electrophysiology (PME) model*. We assume transversely-isotropic electrical conduction, and thus define the normalized conductivity tensor as

$$\boldsymbol{D} = d_{\text{trans}}\boldsymbol{I} + (d_{\text{long}} - d_{\text{trans}})\boldsymbol{n} \otimes \boldsymbol{n},$$

where $d_{\text{trans}}, d_{\text{long}}$ are the normalized conductivities in the transversal and longitudinal directions of the fiber, respectively, and $\boldsymbol{n}$ is the fiber normal vector. For the case of the standard cable model with linear diffusion, as considered in (2.4), typical values for human cardiac tissue are $d_{\text{trans}} = 0.012576\,\text{mm}^2/\text{ms}$ and $d_{\text{long}} = 0.0952\,\text{mm}^2/\text{ms}$. However, we

note here that in the case of the porous-medium diffusion law, the conductivities d_{trans} and d_{long} do not necessarily take on the same values reported in the literature for the standard diffusion models, and therefore conduction velocity tests must be conducted in order to determine their values.

Governing equations (2.2) and (2.3) are complemented with Dirichlet and Neuman boundary conditions,

$$\phi = \bar{\phi}, \quad (\boldsymbol{x}, t) \in \partial\Omega_\phi \times [0, T], \tag{2.6}$$

$$\boldsymbol{q} \cdot \boldsymbol{n} = \bar{q}, \quad (\boldsymbol{x}, t) \in \partial\Omega_q \times [0, T], \tag{2.7}$$

respectively, as well as initial conditions

$$\phi(\boldsymbol{x}, 0) = \phi_0(\boldsymbol{x}), \quad \boldsymbol{x} \in \Omega,$$

$$\boldsymbol{r}(\boldsymbol{x}, 0) = \boldsymbol{r}_0(\boldsymbol{x}), \quad \boldsymbol{x} \in \Omega.$$

In this work, we have chosen the Aliev-Panfilov phenomenological model (Aliev & Panfilov, 1996) which considers one recovery variable r and the following expressions for the ionic current and kinetics:

$$f(\phi, r) = c_1\phi(\phi - \alpha)(1 - \phi) - c_2\phi r\,, \tag{2.8}$$

$$g(\phi, r) = [\gamma + r\bar{\gamma}(\phi)][-r - c_1\phi(\phi - b - 1)]\,, \tag{2.9}$$

with

$$\bar{\gamma}(\phi) = \frac{\mu_1}{\mu_2 + \phi}.$$

The Aliev-Panfilov model has the advantage of being a simple and computationally-tractable celullar model that can be easily incorporated in organ-level simulations (Hurtado & Kuhl, 2014). Further, it has been shown to capture correct restitution curves, while keeping the number of parameters to a small number (Aliev & Panfilov, 1996). The parameter values for the Aliev-Panfilov model employed in all simulations are detailed in

Table 2.1. It is important to remark that some parameters have been adjusted and differ from the original values in order to obtain a correct initial maximum slope of the action potential of $230\,\mathrm{mV/ms}$ typically in human ventricular cardiomyocytes (Drouin, Charpentier, Gauthier, Laurent, & Le Marec, 1995). The initial-boundary value problem just

Table 2.1. Parameter values considered for the Aliev-Panfilov model of ionic current

α	c_1	c_2	μ_1	μ_2	b	γ
0.05	52	8	0.1	0.3	0.25	0.002

described is solved by means of a numerical discretization based on a nonlinear implicit finite-element formulation (Göktepe & Kuhl, 2009; Hurtado & Henao, 2014). The details of the numerical scheme developed to integrate the governing equations proposed for this model can be found in Appendix A.

2.2.2. Simplified cardiac-tissue models

To study the fundamental electrophysiological properties of the proposed PME model, we have first considered a 1-D cardiac fiber with a length of 20 mm. In such model, the transverse area has been considered to be constant and unitary. The corresponding finite element model considered an element size of $\Delta x = 0.01\,\mathrm{mm}$ and a time step size of $\Delta t = 0.01\,\mathrm{ms}$ to ensure that the measured conduction velocity does not have a dependence on the mesh size. Prescribed flux boundary conditions have been considered for both ends of the cardiac fiber, with the right having a zero-flux boundary condition at all times. In the case of the PME model, the normalized conductivities for each value of the m-parameter are fitted in order to obtain a 1-D conduction velocity of $42.7\,\mathrm{cm/s}$. To elicit an action potential, the left end of the fiber was stimulated with an electrical current of $2,100\,\mu\mathrm{A/cm^3}$ for $2\,\mathrm{ms}$. For the case of standard linear diffusion ($m = 0$), we considered a normalized conductivity of $0.0952\,\mathrm{mm^2/ms}$, in line with the values assumed for the longitudinal direction along the fiber. To assess the arrhythmogenic properties of

the PME model, restitution curves for the action-potential duration (APD) and conduction velocity (CV) were generated and compared with the linear diffusion case. To this end, a standard pacing down protocol (Bueno-Orovio et al., 2008) was adopted.

To study the three - dimensional features of the electrical propagation of the PME model, a cuboid cardiac tissue model frequently used as a benchmark (Niederer et al., 2011) was generated. The cuboid has dimensions of $20 \times 7 \times 3\,\mathrm{mm}$, and the domain was discretized using tetrahedral elements with an average edge length of $0.1\,\mathrm{mm}$. Cardiac fibers were oriented in the longest axis direction. A cubic subdomain with dimensions $1.5 \times 1.5 \times 1.5\,\mathrm{mm}$ located at one of the corners of the cuboid was stimulated with an electrical current density of $50,000\,\mu A/cm^3$ for $2\,\mathrm{ms}$. The normalized conductivity constants for the standard diffusion case (m=0) are then amplified according to the conductivity values found in the 1-D case for $m = 4$.

2.2.3. Human biventricular model

A detailed biventricular finite-element model has been constructed based on human heart magnetic-resonance images oriented in the short axis. After a semi-automatic segmentation and smoothing processes, the cardiac muscle was identified and a tetrahedral mesh was created, see Figure 2.2(a). The tetrahedral mesh contains over 1.5 million elements and 320,000 nodes.

The preferential orientation of cardiac myocytes was addressed in this work by defining a fiber orientation at each point of the mesh, and later interpolating the fiber orientation to the integration points. To determine the fiber orientation at all nodes, we have implemented the rule-based algorithm proposed by Bayer, Blake, Plank, and Trayanova (2012), where a series of Laplace problems were solved using a finite-element approach on the mesh shown in Figure 2.2(a). Different Dirichlet boundary conditions were prescribed for the different regions of the biventricular boundary, as indicated by Bayer and co-workers. After some vector operations, a continuous fiber orientation map is recovered, and the fiber vector $\boldsymbol{n}$ was then computed at all nodes of the biventricular mesh. The validation of

this method using diffusion-tensor MRI has been addressed in Bayer et al. (2012). Figure 2.2(b) shows the final 3D reconstruction of the fiber orientation map used in this work.

To account for the His-Purkinje network found in the endocardium of human ventricles, we followed the procedural method developed by Ijiri et al. (2008). In brief, the Purkinje fibers are modeled as an L-system, which is a parallel rewriting system that follows a set of rules specified by the user to create complex branching three-dimensional structures composed by 1-D line elements. The fractal growth process is then pursued on the endocardial surface of the left and right ventricles. It is important to remark that in our model, only the terminals of the generated Purkinje network are connected to cardiac tissue only at the endocardium, following the anatomical observations made in healthy hearts (Pullan et al., 2005). Figure 2.2(c) shows the Purkinje network generated for our biventricular geometry.

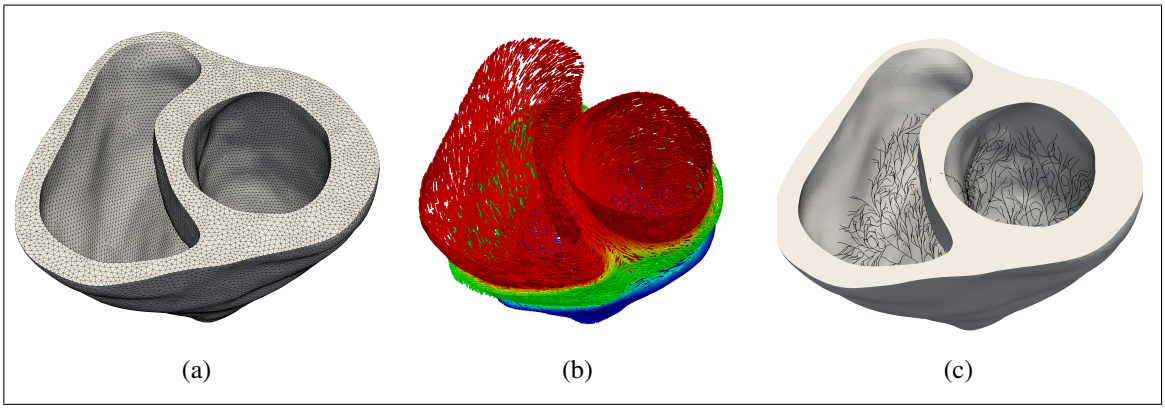

Figure 2.2. Three-dimensional human biventricular model: (a) finite-element tetrahedral mesh, (b) cardiomyocyte fiber orientation, and (c) His-Purkinje network.

2.3. Results

2.3.1. 1-D wave propagation, conduction velocity, wave profiles and restitution properties

A single propagating AP resulting from the solution of the PME model was solved for the 1-D cardiac segment using different values of the conductivity, until the propagating wave attained a CV of $42.7\,\mathrm{cm/s}$, measured at the center of the segment. For all values of m, the AP wavefront was considered to reach a point whenever the normalized voltage value at that point was equal to $\phi = 0.1$ (10% of the AP amplitude), which is above the usual threshold values defined for onset of an AP in several electrophysiology models. The resulting conductivites are summarized in Table 2.2, where it can be observed that PME conductivities are always greater than the conductivity value typically considered for the cable model. The wavefront and waveback for a single propagating AP as dictated by the

Table 2.2. Longitudinal and transversal conductivities for the cable model and the PME model using different exponent values.

	$m = 0$ (Cable)	$m = 1$	$m = 2$	$m = 3$	$m = 4$
d_{long} $[\mathrm{mm}^2/\mathrm{ms}]$	0.0953	0.2037	0.3525	0.5440	0.7803
d_{trans} $[\mathrm{mm}^2/\mathrm{ms}]$	0.0126	0.0269	0.0465	0.0718	0.1030

cable model ($m = 0$) and four cases of the PME model ($m = 1, 2, 3, 4$) can be observed in Figures 2.3(a) and 2.3(b). For the wavefront, all waves coincide at a normalized potential value of $\phi = 0.1$ for the same simulation time, and we observe that there is a sustancial difference in shapes between the cable model and the PME model. First, the cable model results in a Gaussian profile with a long front tail that extends infinitely ahead of the wavefront, as expected from theory. In contrast, for all the PME cases the wave has a sharper front, with steepness increasing with higher m-power values. While the PME waves sharply reach the resting potential at around $X = 10$, the cable-model smoothly tends to $\phi = 0$ far to the right of $X = 10$. The inset of Figure 2.3(a) shows the normalized potential values in logarithmic scale for the region ahead of the wavefront, from which we

observe that the cable wave displays an exponential decay, whereas the PME wave takes the null value for all practical purposes ($\phi < 10^{-60}$ in that region). We have measured the distance between the wavefronts of cases $m = 0$ and $m = 4$ for $\phi = 0.7$, and found that the cable wavefront lags behind the PME wavefront, with spatial gaps that can be as high as $0.6\,\mathrm{mm}$. The comparison of the waveback can be found in Figure 2.3(b), where it can be observed that the PME model results in a steeper waveback as the m-exponent increases. We have also examined the rear-tail behavior away from the AP wave (see inset in Figure 2.3(b)) and found that the PME waves do approach $\phi = 0$ two orders of magnitude faster than the cable-model wave.

The APD and CV restitution curves obtained from the simulation of the 1-D cardiac segment are included in Figure 2.4(a) and 2.4(b). For the case of the APD restitution curve, no significant differences are observed among the standard cable and the PME models. For the CV restitution curves, the shape is the same in all cases, but for a fixed cycle-length, CV may differ by at most $1\,\mathrm{cm/s}$ depending on the model considered. No clear trend is observed as the $m-$exponent is changed.

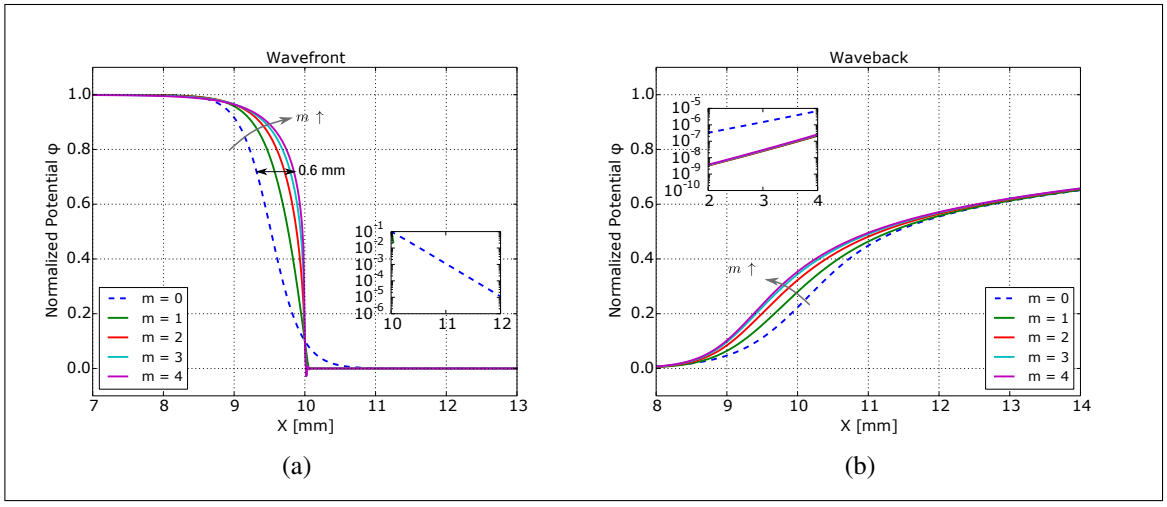

Figure 2.3. Comparison of wave profiles for the 1-D PME model using different $m-$exponent values and the cable model $(m = 0)$. (a) Wavefront and (b) waveback. Insets show a close-up of regions in semilog scale ahead (a) and behind (b) the propagating wave.

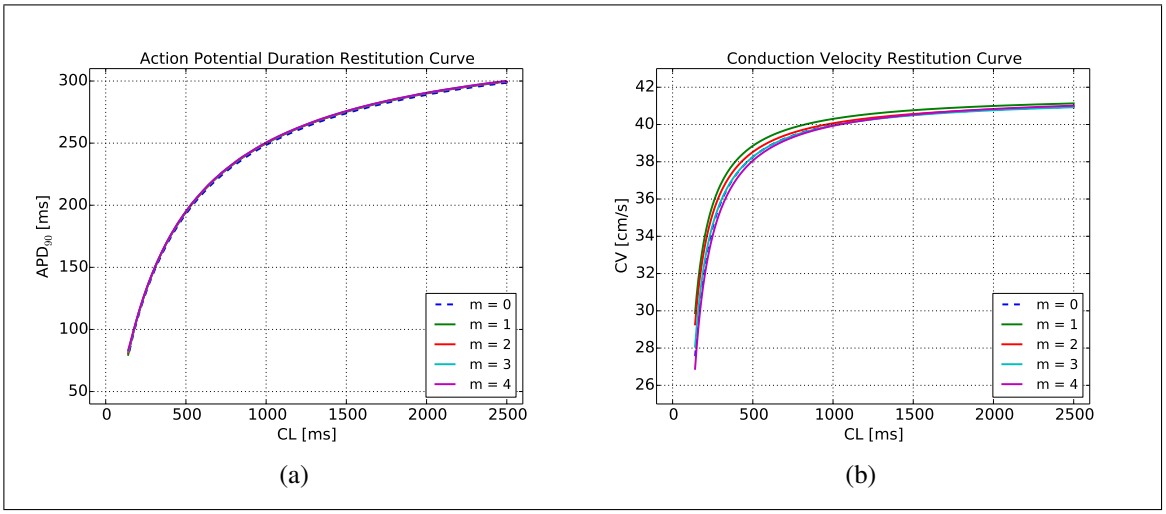

Figure 2.4. APD and conduction velocicty restitution curves. The case $m = 0$ represents the standard linear-diffusion model. Nomenclature: CL = cycle length.

2.3.2. Three-dimensional propagation in a cardiac slab

Figure 2.5 shows the normalized potential distribution for the three-dimensional slab of cardiac tissue described in Section 2.2.2 using a PME model with $m = 4$ and with conductivities as detailed in Table 2.2, for a time instant of $20\,\mathrm{ms}$ after the initial excitation of the cardiac tissue at the bottom left corner. The propagating wavefronts display an ellipsoidal shape, which is in line with the observed features of propagating wavefronts obtained from cable models. We also observe that the ellipsoid's longest axis is aligned with the direction of the assigned cardiac fibers.

To understand the wavefront differences of the PME model with the cable model, we have computed the normalized potential distribution in the slab top surface as predicted by both models for the same time instant, see Figure 2.6. Similar to the 1-D case, the PME wave ends sharply into the resting potential condition, while the cable wave smoothly (exponentially) decays to the resting potential. While both models result in wavefronts with ellipsoidal shape and similar local propagation directions, we observe from the level sets

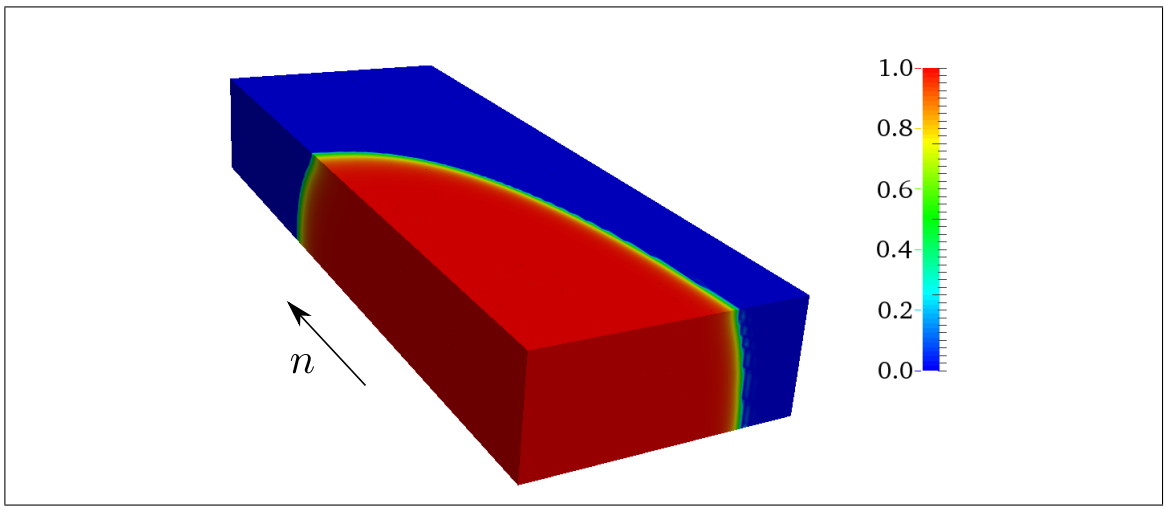

Figure 2.5. PME wave $(m = 4)$ propagating in a cardiac slab. An ellipsoidal wavefront propagates in the three-dimensional medium, with the major axis being aligned with the cardiac fibers in the long-axis direction.

marked in Figure 2.6 that the cable-wave crest-to-trough length is 50% larger than the PME crest-to-trough length. We do observe, however, that the distance between wavefronts $\phi = 0.9$ and $\phi = 0.5$ are very similar for both models. We also observe that level sets in the cable model are very smooth for all normalized potential values, while in the PME model small oscillations may arise in a small and bounded region ahead of the wavefront.

2.3.3. Biventricular human heart PME model activation

Figure 2.7 shows the activation sequence of the ventricles of a human heart using the PME model with an exponent $m = 2$ for a time series with increments of $20\,\mathrm{ms}$. The excitation starts at the atrioventricular node, and propagates through tissue and the His-Purkinje network down the septum, predominantly in the apico-basal direction.The His-Purkinje system rapidly conducts the electrical impulse on the endocardium, from where activation spreads at the network terminals inside the myocardium. The random location of terminals on the endocardium produces a non-smooth and highly anisotropic wavefront. Conduction velocity in the His-Purkinje was verified to be 3-4 times faster than

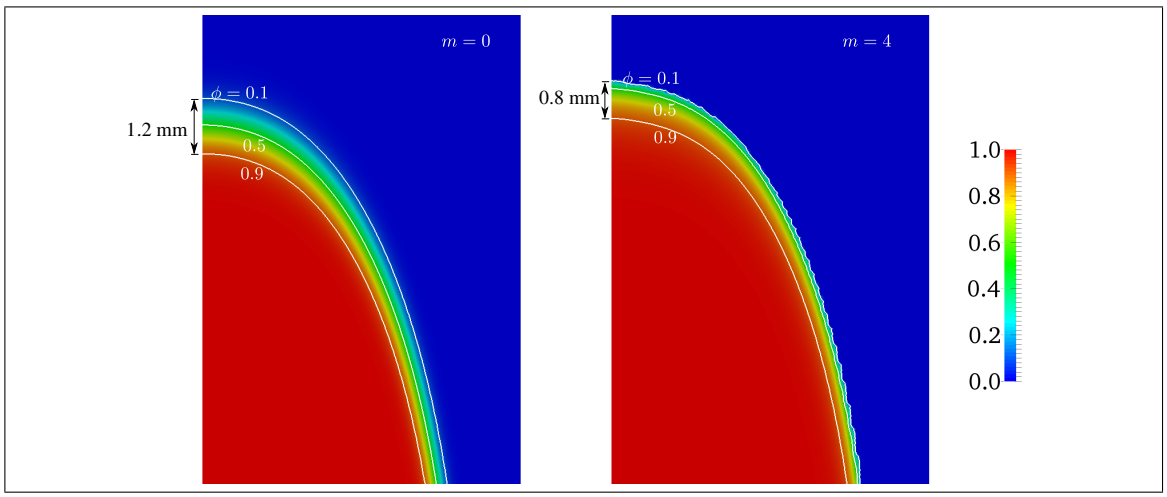

Figure 2.6. Comparison of the normalized potential wavefronts on the top surface for the cable model (left, $m = 0$) and the PME model (right, $m = 4$) in a region of the 3D cardiac slab. Selected level sets are marked in white solid lines.

conduction velocity in cardiac tissue. The total activation sequence takes approximately $120\,\mathrm{ms}$ to fully activate all regions of the ventricular chambers, which is within the time range of normal ventricular depolarization times (Klabunde, 2005).

2.4. Discussion

In this work, we propose a novel cardiac electrophysiology model that features a non-linear diffusion term for the study of the propagation of electrical waves through excitable media. The microstructural features of cardiac conductive tissue, like the porous-membrane structure of intercalated discs, is taken into account in the proposed model by replacing the spatial flux term of the standard cable equations by a porous-medium diffusive term that better reflects the propagation nature of electrical waves at the cellular level while being suitable for tissue- and organ-level simulations.

We have tested the PME model in simplified domains to assess its electrophysiological properties and compare them to those found in the standard cable model. In all the cases considered in this work, the PME model resulted in propagating waves with a well-defined

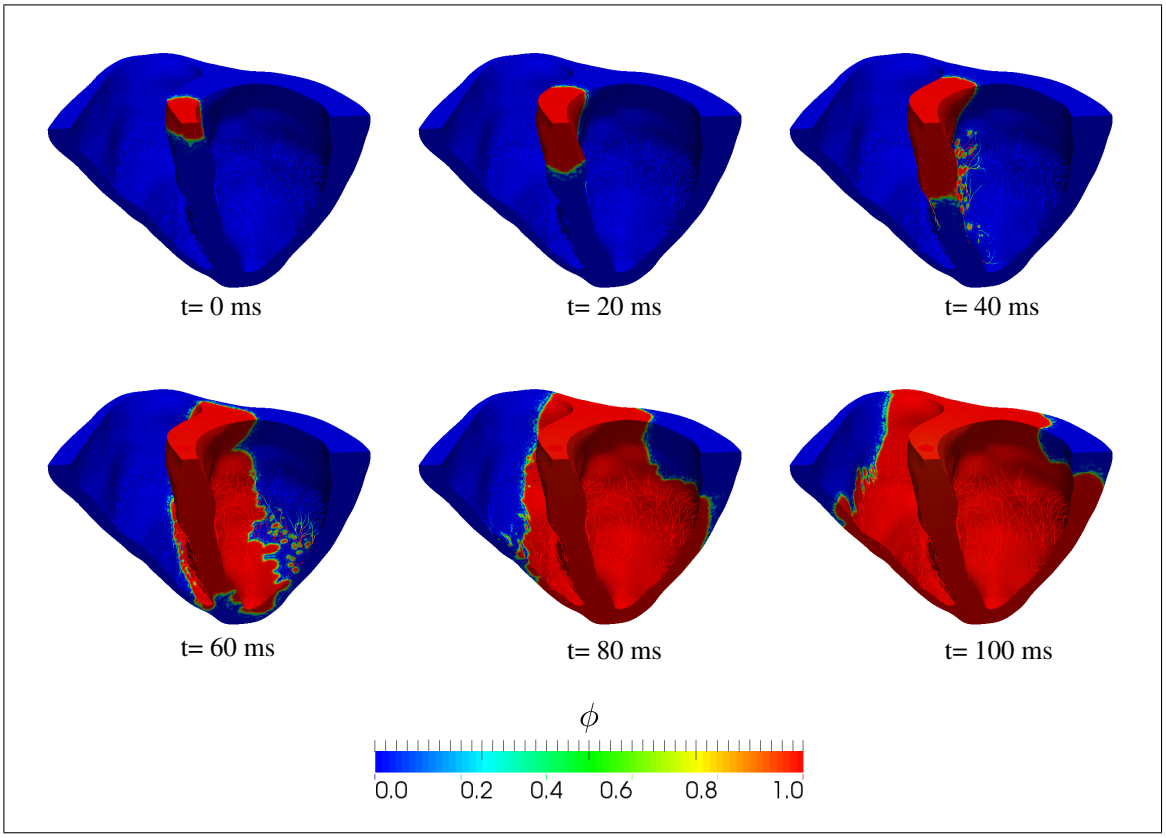

Figure 2.7. Activation sequence of a human biventricular domain using the PME model (m=2). Only half of the biventricular domain is shown for clarity.

and sharp wavefront for which a finite propagation speed could be determined, and for which tissue ahead of the wavefront displays a resting potential. This finding is in contrast with the propagating waves arising from the cable equation, where the wavefront decreases asymptotically to the resting potential, making it difficult to precisely define the wave velocity and wavefront. The m-exponent in the PME model was found to modulate both the front and back of the action potential wave, with higher exponents resulting in steeper wavefronts and wavebacks. The arrhythmogenic properties of the PME model were also analyzed through the construction of APD and CV restitution curves from the 1-D model. No marked differences were found when comparing the PME model curves with those coming from the standard cable model, and therefore we conclude that the PME capture

the restitution properties of cardiac tissue in the same way models based on the cable equation do.

Three-dimensional studies on a cardiac slab showed that the PME model is able to incorporate anisotropic wave propagation. In particular, for a transversely-isotropic tissue architecture we recover ellipsoidal wavefronts similar to those produced by the cable model. Along the principal direction of propagation, PME waves exhibit a crest-to-trough length that is 33% shorter than the cable wave, for the highest $m-$exponent studied in this work. Similar to the 1-D case, the wavefront in the PME model has a well defined location, with tissue ahead of the wavefront that exactly takes on the resting potential value.

The spatio-temporal differences introduced by the PME model suggest important implications concerning repolarization dynamics and morphology. The modifications of the wavefront and waveback dynamics are in fact tightly linked with several pathological conditions known in cardiac tissue electrophysiology leading to sudden cardiac death, e.g. Brugada syndrome (Brugada, Brugada, & Roy, 2013). Moreover, dispersion of repolarization in larger portions of the heart (Coronel, Wilms-Schopman, Opthof, & Janse, 2009), and in the ventricular wall in particular, have been shown to be an important factor leading to the onset of arrhythmias both in healthy and diseased hearts, as well as to represent the key element for sustained fibrillation scenarios (Fenton, Cherry, Hastings, & Evans, 2002). Thus, the differences in wavefront and waveback steepness open novel interesting questions about the spatio-temporal dispersion of repolarization characters that we propose to explored via the PME model formulation. The constitutive nonlinear flux assumption, in fact, introduces an additional multiscale feedback in the membrane potential dynamics.

Finally, we have demonstrated that the PME model is amenable to large-scale 3D whole-heart simulations. In particular, activation sequences in the human ventricles can be simulated using the PME model, in which the heterogeneous fiber orientation of cardiomyocytes can be incorporated in a similar fashion standard cable models incorporate anisotropic conduction. The PME model for cardiac tissue works well when coupled with

a 1-D His-Purkinje network, which is fundamental to better reflect the ventricular activation that mainly starts at the terminals embedded in the endocardium. The resulting wavefront is non-smooth and heterogeneous, which reflects well the experimental observations of the propagation of action potentials, as found in optical mapping experiments (Gizzi et al., 2013). We conclude that the PME model is amenable to simulations in realistic cardiac geometries and well suited for applications in the study of excitation in complex heterogeneous and anisotropic biological media.

2.4.1. Limitations and Outlook

From a physiological point of view, one limitation of this work is the admittedly simple electrophysiological model adopted. The reason for adopting a phenomenological model with a simple AP morphology was to avoid the highly complex dynamics that a biophysical ionic model introduces into the simulation, and thus concentrate on the effects of the non-linear diffusion term introduced in this work. In a forthcoming contribution, we plan to validate our generalized approach using well-established phenomenological (Bueno-Orovio et al., 2008) and biophysical cardiac ionic models (Clayton et al., 2011), in order to quantify the sensitivity of realistic models with respect to the nonlinear diffusion flux of the PME model. With better ionic models, one objective is the study of the onset of arrhythmias and the different fibrillation scenarios (Cherry & Fenton, 2008) and how these phenomena are affected by the non-linear diffusion flux in terms of wavefront steepening and wave tail fastening as the key features of the PME formulation. A deeper understanding of the possible effects linked to finite speed wave propagation can also be explored in direct comparison with experimental evidences. Qualitative and quantitative analysis addressing spatio-temporal alternans dynamics and conduction blockage that aim at reproducing such complex behaviors not fully recovered by the current cable-like mathematical formulations are certainly another interesting avenue of research.

From a numerical analysis viewpoint, we consistently found oscillations in a small region ahead of the wavefront that quickly dissipates for regions farther ahead from the

wavefront. Oscillations and their magnitude were highly dependant on the mesh size, and for meshes with characteristic lengths in the order of $0.1\,\mathrm{mm}$ were found to be negligible, as can be seen in 1-D simulations. The existence of small oscillations, which are not found in the cable model, are a purely numerical artefact that can be explained by loss of symmetry of the weak form due to the existence of a convective term, a feature not present in standard linear-diffusion problems (Donea & Huerta, 2003). In the future, we plan to use Petrov-Galerkin schemes that stabilize oscillations, but that may increase the computational efforts needed to solve the PME model. Another important point to remark is that the numerical solution of the PME model takes longer computing times than the solution of the cable model. This additional computing time is attributed to the fact that, when solving for the current state inside an iteration of the implicit scheme adopted, a non-symmetric linear system must be solved in the PME model, in contrast with the symmetric linear system that was found for the cable model using the Aliev-Panfilov ionic current. Thus, efficient algorithms commonly used to solve symmetric linear systems do not apply for the case of the PME equation. This additional cost may be drastically reduced when considering explicit integration schemes, at the expense of smaller time steps that are typically constrained by the mesh size.

Bioengineering computational applications of the PME model can be extended to multiphysics problems, not limited to the sole electrical excitation of cardiac tissue. We expect that the PME formulation can be applied to a wide range of excitable syncytia spanning from single cell excitation-contraction and cell-to-cell dynamics (Ruiz-Baier et al., 2014) to thermo-electro-mechanic tissue and organ models (Filippi, Gizzi, Cherubini, Luther, & Fenton, 2014; Cookson et al., 2012; Huyghe et al., 1992; Altomare et al., 2014). In conclusion, we propose the PME model approach as a possible and reliable theoretical generalization of the classical electrophysiological cable model that could open new perspectives in the mathematical modeling of complex biological excitable media.

3. CONCLUSIONS

In the present work, the standard flux term for the monodomain model is changed by a porous-medium diffusive term. This change, as expected, provides a more physical solution with respect the propagation of the wavefront through the cardiac cells.

As said in Chapter 1, the porous medium equation has the advantage to recover a finite speed in the wavefront, on the contrary that the standard monodomain model. In order to analyze the changes obtained with the PME model we have run simulations in simplified domains. We note that, as expected, the action potencial after the wavefront is equal to zero in the PME model but positive in the standard cable model. In addition, analyzing how the $m-$exponent affects to the wavefront, we note that using a higher value for m the wavefront is steepter. However, these changes do not affect to the arrhythmogenic properities as the APD and CV restitution curves from the 1-D model. The same analysis is made in a three-dimensional cardiac slab, considering an anisotropic diffusion. As like the 1-D case, the wavefront in the PME is well defined along all directions.

Finally, we run 3D simulations in a whole-heart, studying the activation sequence in the human ventricles. We can see that the PME model works well for the cardiac tissue coupled with the His-Purkinje network and the myocardial fibers. The wavefront recovers well the experimental observations of the propagation of action potentials. We conclude that the PME model is suitable for simulations in realistic geometries.

4. FUTURE WORK

The topic addressed in the present work is strongly multidisciplinar and open several perspectives of improvement. Some ideas are listed below.

The first point to analyze is the limitation imposed by the phenomenological model employed in this work. A straightforward extention of the present work consists in fact in analyzing the PME formulation in a more sotisficated models as exposed in Chapter 1. For example the Minimal model (Bueno-Orovio et al., 2008) or the ten Tusscher model (ten Tusscher et al., 2004) arise as good candidates as more accurate ionic models. Specific studies would then address the onset of arrhythmias and the different fibrillation scenarios (Cherry & Fenton, 2008) and how these phenomena are affected by the non-linear diffusion flux in terms of wavefront steepening and wave tail fastening as the key features of the PME formulation. Moreover, deeper analysis of the effects of the finite speed wave propagation can also be made, in comparison of experimental results.

From a numerical point of view there are several options to improve the present work. The first one is about the oscillations that we found in the wavefront, and that get larger as we increase the $m-$exponent. In order to solve this problem we foresee the analysis of finer meshes or the use of discontinuous finite element methods. If refinement of the mesh is required, an interesting project would consists in refining around the wavefront i.e., to use adaptive mesh refinement, in order to reduce the oscillations without increasing the computational cost. Other options to analyze the non-symmetric system and optimize the computational time required. Explicit schemes, with smaller time step, could be a possible strategy.

The PME model is not limited to the electrical propagation only. This formulation can be extended to multiphysics couplings as the thermo-electro-mechanical problem of the cardiac tissue. Therefore, we foresee a wide applicability of the PME model in the mathematical biology and physiology fields.

REFERENCES

Alberts, B., Johnson, A., Lewis, J., Raff, M., Roberts, K., & Walter, P. (2007). *Molecular biology of the cell*. New York: Garland Science.

Aliev, R. R., & Panfilov, A. V. (1996). A simple two-variable model of cardiac excitation. *Chaos, Solitons & Fractals*, *7*(3), 293 - 301. doi: 10.1016/0960-0779(95)00089-5

Altomare, A., Gizzi, A., Guarino, M. P. L., Loppini, A., Cocca, S., Dipaola, M., ... Filippi, S. (2014). Experimental evidence and mathematical modeling of thermal effects on human colonic smooth muscle contractility. *American Journal of Physiology - Gastrointestinal and Liver Physiology*, *307*(1), G77–G88. doi: 10.1152/ajpgi.00385.2013

Bayer, J., Blake, R., Plank, G., & Trayanova, N. (2012). A novel rule-based algorithm for assigning myocardial fiber orientation to computational heart models. *Annals of Biomedical Engineering*, *40*(10), 2243-2254. doi: 10.1007/s10439-012-0593-5

Bini, D., Cherubini, C., Filippi, S., Gizzi, A., & Ricci, P. E. (2010). On spiral waves arising in natural systems. *Communications in Computational Physics*, *8*(3), 610 - 622. doi: 10.4208/cicp.240909.170210a

Brugada, P., Brugada, J., & Roy, D. (2013). Brugada syndrome 1992–2012: 20 years of scientific excitement, and more. *European Heart Journal*, *34*(47), 3610–3615. doi: 10.1093/eurheartj/eht113

Bueno-Orovio, A., Cherry, E. M., & Fenton, F. H. (2008). Minimal model for human ventricular action potentials in tissue. *Journal of Theoretical Biology*, *253*(3), 544 - 560. doi: 10.1016/j.jtbi.2008.03.029

Bueno-Orovio, A., Kay, D., Grau, V., Rodriguez, B., & Burrage, K. (2014). Fractional diffusion models of cardiac electrical propagation: role of structural heterogeneity in dispersion of repolarization. *Journal of The Royal Society Interface*, *11*(97). doi: 10.1098/rsif.2014.0352

Cherry, E. M., & Fenton, F. H. (2004). Suppression of alternans and conduction blocks

despite steep apd restitution: electrotonic, memory, and conduction velocity restitution effects. *American Journal of Physiology - Heart and Circulatory Physiology*, *286*(6), H2332–H2341. doi: 10.1152/ajpheart.00747.2003

Cherry, E. M., & Fenton, F. H. (2008). Visualization of spiral and scroll waves in simulated and experimental cardiac tissue. *New Journal of Physics*, *10*(12), 125016. doi: 10.1088/1367-2630/10/12/125016

Cherubini, C., Gizzi, A., Bertolaso, M., Tambone, V., & Filippi, S. (2012). A bistable field model of cancer dynamics. *Communications in Computational Physics*, *11*(1). doi: 10.4208/cicp.270710.220211a

Clayton, R., Bernus, O., Cherry, E., Dierckx, H., Fenton, F., Mirabella, L., ... Zhang, H. (2011). Models of cardiac tissue electrophysiology: Progress, challenges and open questions. *Progress in Biophysics and Molecular Biology*, *104*(13), 22 - 48. (Cardiac Physiome project: Mathematical and Modelling Foundations) doi: 10.1016/j.pbiomolbio.2010.05.008

Cookson, A., Lee, J., Michler, C., Chabiniok, R., Hyde, E., Nordsletten, D., ... Smith, N. (2012). A novel porous mechanical framework for modelling the interaction between coronary perfusion and myocardial mechanics. *Journal of Biomechanics*, *45*(5), 850 - 855. (Special Issue on Cardiovascular Solid Mechanics) doi: 10.1016/j.jbiomech.2011.11.026

Coronel, R., Wilms-Schopman, F. J., Opthof, T., & Janse, M. J. (2009). Dispersion of repolarization and arrhythmogenesis. *Heart Rhythm*, *6*(4), 537 - 543. doi: 10.1016/j.hrthm.2009.01.013

Costa, K. D., Hunter, P. J., Wayne, J. S., Waldman, L. K., Guccione, J. M., & McCulloch, A. D. (1996). A three-dimensional finite element method for large elastic deformations of ventricular myocardium: Iiprolate spheroidal coordinates. *Journal of Biomechanical Engineering*, *118*(4), 464-472. doi: 10.1115/1.2796032

Davidenko, J. M., Pertsov, A. V., Salomonz, R., Baxter, W., & Jalife, J. (1992). Stationary and drifting spiral waves of excitation in isolated cardiac. *Nature*, *355*, 349 - 351. doi: 10.1038/355349a0

Demiray, H. (1976). Stresses in ventricular wall. *Journal of Applied Mechanics*, *43*(2), 194-197. doi: 10.1115/1.3423806

Donea, J., & Huerta, A. (2003). *Finite element methods for flow problems*. John Wiley & Sons, Chichester, England.

Drouin, E., Charpentier, F., Gauthier, C., Laurent, K., & Le Marec, H. (1995). Electrophysiologic characteristics of cells spanning the left ventricular wall of human heart: Evidence for presence of m cells. *Journal of the American College of Cardiology*, *26*(1), 185 - 192. doi: 10.1016/0735-1097(95)00167-X

Fenton, F. H., & Cherry, E. M. (2008). Models of cardiac cell. *Scholarpedia*, *3*(8), 1868. doi: 10.4249/scholarpedia.1868

Fenton, F. H., Cherry, E. M., Hastings, H. M., & Evans, S. J. (2002). Multiple mechanisms of spiral wave breakup in a model of cardiac electrical activity. *Chaos: An Interdisciplinary Journal of Nonlinear Science*, *12*(3), 852-892. doi: 10.1063/1.1504242

Fenton, F. H., Gizzi, A., Cherubini, C., Pomella, N., & Filippi, S. (2013, Apr). Role of temperature on nonlinear cardiac dynamics. *Physical Review E*, *87*, 042717. doi: 10.1103/PhysRevE.87.042717

Fenton, F. H., & Karma, A. (1998). Vortex dynamics in three-dimensional continuous myocardium with fiber rotation: Filament instability and fibrillation. *Chaos: An Interdisciplinary Journal of Nonlinear Science*, *8*(1), 20-47. doi: 10.1063/1.166311

Fenton, F. H., Luther, S., Cherry, E. M., Otani, N. F., Krinsky, V., Pumir, A., ... Gilmour, R. F. (2009). Termination of atrial fibrillation using pulsed low-energy far-field stimulation. *Circulation*, *120*(6), 467-476. doi: 10.1161/CIRCULATIONAHA.108.825091

Filippi, S., Gizzi, A., Cherubini, C., Luther, S., & Fenton, F. H. (2014). Mechanistic insights into hypothermic ventricular fibrillation: the role of temperature and tissue size. *Europace*, *16*(3), 424–434. doi: 10.1093/europace/euu031

FitzHugh, R. (1961). Impulses and physiological states in theoretical models of nerve membrane. *Biophysical Journal*, *1*, 445–466. doi: 10.1016/s0006-3495(61)86902-6

Friedman, A. (1964). *Partial differential equations of parabolic type*. Prentice-Hall.

Gizzi, A., Cherry, E., Gilmour, R. F., Luther, S., Filippi, S., & Fenton, F. H. (2013). Effects of pacing site and stimulation history on alternans dynamics and the development of complex spatiotemporal patterns in cardiac tissue. *Frontiers in Physiology*, *4*(71). doi: 10.3389/fphys.2013.00071

Glukhov, A. V., Egorov, Y. V., Efimov, I. R., & Rosenshtraukh, L. V. (2012). Cardiac electrical alternans and ventricular fibrillation during hypothermia in non-hibernating versus hibernating animals: Role of propagation velocity and dispersion of repolarization. In T. Ruf, C. Bieber, W. Arnold, & E. Millesi (Eds.), *Living in a seasonal world* (p. 293-303). Springer Berlin Heidelberg. doi: 10.1007/978-3-642-28678-0_26

Göktepe, S., & Kuhl, E. (2009). Computational modeling of cardiac electrophysiology: A novel finite element approach. *International Journal for Numerical Methods in Engineering*, *79*(2), 156–178. doi: 10.1002/nme.2571

Guccione, J. M., McCulloch, A. D., & Waldman, L. K. (1991). Passive material properties of intact ventricular myocardium determined from a cylindrical model. *Journal of Biomechanical Engineering*, *113*(1), 42-55. doi: 10.1115/1.2894084

Guyton, A., & Hall, J. (2006). *Textbook of medical physiology*. Elsevier Saunders.

Henriquez, C. S. (1993). Simulating the electrical behavior of cardiac tissue using the bidomain model. *Crit. Rev. Biomed. Eng.*, *21*(3), 1 - 77.

Hodgkin, A. L., & Huxley, A. F. (1952). A quantitative description of membrane current and its application to conduction and excitation in nerve. *Journal of Physiology*, *117*(4), 500 - 544. doi: 10.1007/BF02459568

Holzapfel, G. A., & Ogden, R. W. (2009). Constitutive modelling of passive myocardium: a structurally based framework for material characterization. *Philosophical Transactions of the Royal Society A: Mathematical, Physical and Engineering Sciences*, *367*(1902), 3445-3475. doi: 10.1098/rsta.2009.0091

Hurtado, D. E., & Henao, D. (2014). Gradient flows and variational principles for cardiac

electrophysiology: Toward efficient and robust numerical simulations of the electrical activity of the heart. *Computer Methods in Applied Mechanics and Engineering*, *273*(0), 238 - 254. doi: 10.1016/j.cma.2014.02.002

Hurtado, D. E., & Kuhl, E. (2014). Computational modelling of electrocardiograms: repolarisation and t-wave polarity in the human heart. *Computer Methods in Biomechanics and Biomedical Engineering*, *17*(9), 986-996. doi: 10.1080/10255842.2012.729582

Huyghe, J. M., Arts, T., van Campen, D. H., & Reneman, R. S. (1992). Porous medium finite element model of the beating left ventricle. *American Journal of Physiology - Heart and Circulatory Physiology*, *262*(4), H1256–H1267.

Ijiri, T., Ashihara, T., Yamaguchi, T., Takayama, K., Igarashi, T., Shimada, T., ... Nakazawa, K. (2008). A procedural method for modeling the purkinje fibers of the heart. *The Journal of Physiological Sciences*, *58*(7), 481-486. doi: 10.2170/physiolsci.RP003208

Katz, A. (2006). *Physiology of the heart*. Lippincott Williams & Wilkins.

Keener, J., & Sneyd, J. (2008a). *Mathematical physiology: I: Cellular physiology*. Springer New York.

Keener, J., & Sneyd, J. (2008b). *Mathematical physiology: II: Systems physiology*. Springer New York.

Khaled, A.-R., & Vafai, K. (2003). The role of porous media in modeling flow and heat transfer in biological tissues. *International Journal of Heat and Mass Transfer*, *46*(26), 4989 - 5003. doi: 10.1016/S0017-9310(03)00301-6

Klabunde, R. (2005). *Cardiovascular physiology concepts*. Lippincott Williams & Wilkins.

Krishnamurthy, A., Villongco, C. T., Chuang, J., Frank, L. R., Nigam, V., Belezzuoli, E., ... Kerckhoffs, R. C. (2013). Patient-specific models of cardiac biomechanics. *Journal of Computational Physics*, *244*(0), 4 - 21. (Multi-scale Modeling and Simulation of Biological Systems) doi: 10.1016/j.jcp.2012.09.015

Ladyzhenskaia, O. A., Solonnikov, V. A., & Ural'ceva, N. N. (1968). *Linear and quasi-linear equations of parabolic type*. American Mathematical Society.

Leibenzon, L. S. (1930). *The motion of a gas in a porous medium*. Russian Academy of Sciences, Moscow.

Luther, S., Fenton, F. H., Kornreich, B. G., Squires, A., Bittihn, P., Hornung, D., ... Bodenschatz, E. (2011). Low-energy control of electrical turbulence in the heart. *Nature*, *475*(7355), 235 - 239. doi: 10.1038/nature10216

Murray, J. D. (2003). *Mathematical biology*. Springer-Verlag, Berlin.

Muskat, M., & Wyckoff, R. (1937). *The flow of homogeneous fluids through porous media*. McGraw-Hill Book Company, Incorporated.

Nagumo, J., Arimoto, S., & Yoshizawa, S. (1962, Oct). An active pulse transmission line simulating nerve axon. *Proceedings of the IRE*, *50*(10), 2061-2070. doi: 10.1109/JRPROC.1962.288235

Niebur, E. (2008). Neuronal cable theory. *Scholarpedia*, *3*(5), 2674. doi: 10.4249/scholarpedia.2674

Niederer, S. A., Kerfoot, E., Benson, A. P., Bernabeu, M. O., Bernus, O., Bradley, C., ... Smith, N. P. (2011). Verification of cardiac tissue electrophysiology simulators using an n-version benchmark. *Philosophical Transactions of the Royal Society A: Mathematical, Physical and Engineering Sciences*, *369*(1954), 4331-4351. doi: 10.1098/rsta.2011.0139

Nordsletten, D., Niederer, S., Nash, M., Hunter, P., & Smith, N. (2011). Coupling multi-physics models to cardiac mechanics. *Progress in Biophysics and Molecular Biology*, *104*(13), 77 - 88. (Cardiac Physiome project: Mathematical and Modelling Foundations) doi: 10.1016/j.pbiomolbio.2009.11.001

Oleinik, O. A., Kalashnikov, A. S., & Juj-lin, C. (1958). The cauchy problem and boundary problems for equations of the type of non-stationary filtration. *Izv. Akad. Nauk SSSR Ser. Mat.*, *22*(5), 667 - 704.

Pavliotis, G., & Stuart, A. (2008). *Multiscale methods: Averaging and homogenization*. Springer.

Pullan, A. J., Cheng, L. K., & Buist, M. L. (2005). *Mathematically Modeling the Electrical Activity of the Heart: From Cell to Body Surface and Back Again*. World Scientific Publishing Company. Hardcover.

Ruiz-Baier, R., Gizzi, A., Rossi, S., Cherubini, C., Laadhari, A., Filippi, S., & Quarteroni, A. (2014). Mathematical modelling of active contraction in isolated cardiomyocytes. *Mathematical Medicine and Biology*, *31*(3), 259-283. doi: 10.1093/imammb/dqt009

Schmid, H., & Hunter, P. J. (2009). Multi-scale modelling of the heart. In G. Holzapfel & R. Ogden (Eds.), *Biomechanical modelling at the molecular, cellular and tissue levels* (Vol. 508, p. 83-177). Springer Vienna. doi: 10.1007/978-3-211-95875-9_2

Schmid, H., Nash, M. P., Young, A. A., & Hunter, P. J. (2006). Myocardial material parameter estimationa comparative study for simple shear. *Journal of Biomechanical Engineering*, *128*(5), 742-750. doi: 10.1115/1.2244576

Severs, N. J., Bruce, A. F., Dupont, E., & Rothery, S. (2008). Remodelling of gap junctions and connexin expression in diseased myocardium. *Cardiovascular Research*, *80*(1), 9–19. doi: 10.1093/cvr/cvn133

Smoller, J. (1982). *Shock waves and reaction-diffusion equations*. New York: Springer-Verlag.

Spach, M. S., Heidlage, J. F., Dolber, P. C., & Barr, R. C. (1998). Extracellular discontinuities in cardiac muscle: Evidence for capillary effects on the action potential foot. *Circulation Research*, *83*(11), 1144-1164. doi: 10.1161/01.RES.83.11.1144

Spach, M. S., Miller, W. T., Geselowitz, D. B., Barr, R. C., Kootsey, J. M., & Johnson, E. A. (1981). The discontinuous nature of propagation in normal canine cardiac muscle. evidence for recurrent discontinuities of intracellular resistance that affect the membrane currents. *Circulation Research*, *48*(1), 39-54. doi: 10.1161/01.RES.48.1.39

ten Tusscher, K. H. W. J., Noble, D., Noble, P. J., & Panfilov, A. V. (2004). A model for human ventricular tissue. *American Journal of Physiology - Heart and Circulatory Physiology*, *286*(4), H1573–H1589. doi: 10.1152/ajpheart.00794.2003

Tung, L. (1978). *A bi-domain model for describing ischemic myocardial d-c potentials* (Unpublished doctoral dissertation). Massachussets Institute of Technology, Cambridge, MA.

Turing, A. M. (1952). The chemical basis of morphogenesis. *Philosophical Transactions of the Royal Society of London. Series B, Biological Sciences*, *237*(641), 37-72. doi: 10.1098/rstb.1952.0012

Vasquez, J. L. (2006). *The porous medium equation*. Oxford University Press, USA. doi: 10.1093/acprof:oso/9780198569039.001.0001

Vazquez, J. L. (1992). An introduction to the mathematical theory of the porous medium equation. In M. Delfour & G. Sabidussi (Eds.), *Shape optimization and free boundaries* (Vol. 380, p. 347-389). Springer Netherlands. doi: 10.1007/978-94-011-2710-3_10

Watanabe, M. A., Fenton, F. H., Evans, S. J., Hastings, H. M., & Karma, A. (2001). Mechanisms for discordant alternans. *Journal of Cardiovascular Electrophysiology*, *12*, 196 - 206. doi: 10.1046/j.1540-8167.2001.00196.x

Winfree, A. (1987). *When time breaks down: The three-dimensional dynamics of electrochemical waves and cardiac arrhythmias*. Princeton University Press.

Winfree, A. (2001). *The geometry of biological time*. Springer New York.

Zeldovich, I. A. B., & Raizer, I. U. P. (1966). *Physics of shock waves and high-temperature hydrodynamic phenomena*. New York: Academic Press.

APPENDIX

A. SPATIO-TEMPORAL DISCRETIZATION: NON-LINEAR IMPLICIT FINITE-ELEMENT FORMULATION

We start by considering a partition of the time interval $[0, T]$ into $\mathrm{n_{stp}}$ subintervals $[t_n, t_{n+1}]$ such that $t_0 = 0$, $t_{\mathrm{n_{stp}}} = T$ and $[0, T] = \bigcup_{n=1}^{\mathrm{n_{stp}}-1} [t_n, t_{n+1}]$. For a generic subinterval $[t_n, t_{n+1}]$ we define $\Delta t = t_{n+1} - t_n$, and assume that the field $\phi_n(\boldsymbol{x}) = \phi(\boldsymbol{x}, t_n)$ is known at $t = t_n$, and look to solve for $\phi_{n+1}(\boldsymbol{x})$. For the sake of simplicity, in the following we omit the index $(\circ)_{n+1}$ of the current time field of interest, i.e. $\phi_{n+1} \equiv \phi$. Adopting a backward Euler time integration scheme for the temporal discretization, we approximate time derivatives by

$$\dot{\phi} \approx \frac{\phi - \phi_n}{\Delta t}, \tag{A.1}$$

$$\dot{r} \approx \frac{r - r_n}{\Delta t}. \tag{A.2}$$

We now focus on the numerical approximation of the evolution equation for the recovery variable. We note that (2.3) depends only locally on ϕ and does not involve spatial gradients. Therefore, we solve the time integration pointwise using a standard backward Euler scheme for (2.3) which results in

$$\mathsf{R}^r = r - r_n - \Delta t\, g(\phi, r) = 0. \tag{A.3}$$

Given a fixed value of ϕ, we use a Newton iteration to solve (A.3), and therefore we require to compute its tangent, which is given by

$$D\mathsf{R}^r = \frac{\partial \mathsf{R}^r}{\partial r} = 1 - \Delta t\, \frac{\partial g}{\partial r}(\phi, r) = 0. \tag{A.4}$$

Thus, given an initial guess for r, we recursively update the recovery variable $r \leftarrow r - (D\mathsf{R}^r)^{-1}\mathsf{R}^r$ until a convergence criteria based on the residual norm is met. The converged value of the recovery variable is denoted $r^*(\phi)$. We denote the algorithm just described is general for any cellular electrophysiology model. We will also be interested in the sensitivity of the recovery variable with respect to the potential variable. Observing that

$r^*(\phi)$ satisfies (A.3), we use implicit differentiation to obtain

$$\frac{\mathrm{d}r^*}{\mathrm{d}\phi}(\phi) = -(D\mathsf{R}^r)^{-1}\left(\frac{\partial g}{\partial \phi}\right)\Big|_{\phi, r^*(\phi)} \tag{A.5}$$

Finally, for the particular case of the Aliev-Panfilov model, we have (Göktepe & Kuhl, 2009)

$$\mathsf{R}^r = r - r_n - [\,[\,\gamma + r\,\bar{\gamma}\,]\,[\,-r - c\,\phi\,[\phi - b - 1]]\,]\Delta t, \tag{A.6}$$

$$D\mathsf{R}^r = 1 + [\gamma + \bar{\gamma}(\phi)\,[\,2\,r + c\,\phi\,[\phi - b - 1]\,]\,]\,\Delta t \tag{A.7}$$

$$\frac{\partial g}{\partial \phi} = [[\gamma + r\,\bar{\gamma}(\phi)]\,c\,[\,2\phi - b - 1\,] + r\,\frac{\partial \bar{\gamma}}{\partial \phi}[\,r + c\,\phi\,[\,\phi - b - 1\,]]\,]\Delta t \tag{A.8}$$

with

$$\frac{\partial \bar{\gamma}}{\partial \phi} = -\frac{\mu_1}{(\mu_2 + \phi)^2}.$$

We now turn our attention to the spatial discretization of equation (2.2) using an electric flux of the kind (2.5). To this end, we start by constructing the weak form of the PME problem. With a slight abuse of notation, let $\phi : \Omega \to \mathbb{R}$ be a trial function satisfying the Dirichlet boundary condition (2.6), and $\delta\phi : \Omega \to \mathbb{R}$ be a test function satisfying $\delta\phi\Big|_{x \in \partial\Omega_\phi} = 0$. By multiplying equation (2.2) by an arbitrary test function $\delta\phi$, integrating it over the domain Ω, applying the standard integration by parts, and including the Neumann boundary conditions (2.7), we arrive at the following weak form:

find ϕ such that

$$\int_\Omega \left\{\dot{\phi}\delta\phi - \boldsymbol{q}(\phi, \nabla\phi)\cdot\nabla\delta\phi - f(\phi, r)\delta\phi\right\} d\boldsymbol{x} + \int_{\partial\Omega_q} \bar{q}\delta\,\phi dS = 0, \quad \forall\delta\phi. \tag{A.9}$$

We now proceed to approximately solve (A.9) using a finite-element approach. To this end, we consider a discretization $\Omega^h \subset \Omega$ which is composed by finite-element domains Ω^e such that $\Omega^h = \bigcup_{e=1}^{\mathrm{n_{el}}} \Omega^e$. Trial functions $\phi^h : \Omega^h \times [0, T] \to \mathbb{R}$ and test functions

$\delta\phi^h : \Omega^h \to \mathbb{R}$ are defined as

$$\phi^h(\boldsymbol{x},t)\big|_{\Omega^e} = \sum_{a=1}^{\mathrm{n_{em}}} N_a^e(\boldsymbol{x})\,\phi_a(t), \tag{A.10}$$

$$\delta\phi^h(\boldsymbol{x})\Big|_{\Omega^e} = \sum_{a=1}^{\mathrm{n_{em}}} N_a^e(\boldsymbol{x})\delta\,\phi_a \tag{A.11}$$

respectively, where $N_a^e(\boldsymbol{x})$ is the element shape function, ϕ_a the trial function nodal value and $\delta\phi_a$ the test function nodal value defined for all element nodes $a = 1,\dots,\mathrm{n_{em}}$. In this particular work, linear isoparametric shape functions on tetrahedral elements are employed, but the formulation here described is general, and can be used for other basis functions. For the generic time interval $[t_n, t_{n+1}]$, we substitute temporal (A.1) and spatial (A.10), (A.11) discretizations into the weak form (A.9) to obtain a set of equations of the form

$$\begin{aligned}\mathsf{R}_A^\phi = \mathbb{A}_{e=1}^{\mathrm{n_{el}}} \int_{\Omega^e} \left\{ N_a^e \frac{\phi^h - \phi_n^h}{\Delta t} - \nabla N_a^e \cdot \boldsymbol{q}(\phi^h, \nabla\phi^h) - N_a^e\, f(\phi^h, r^*) \right\} d\boldsymbol{x} \\ + \int_{\partial\Omega_q^e} N_a^e\, \bar{q}\, dS = 0\end{aligned} \tag{A.12}$$

where the assembly operator $\mathbb{A}$ adds the element contributions at the element nodes $a = 1,\dots,\mathrm{n_{en}}$ to the global residual at the global nodes $A = 1,\dots,\mathrm{n_{nd}}$. The set of non-linear equations implied in (A.12) are commonly solved using gradient-descent iterative schemes, for which the tangent may be required. A straightforward calculation yields the following expression for the tangent components

$$\begin{aligned}D\mathsf{R}_{AB}^\phi = \frac{\partial \mathsf{R}_A^\phi}{\partial \phi_B} = \mathbb{A}_{e=1}^{\mathrm{n_{el}}} \int_{\Omega^e} \left\{ \frac{1}{\Delta t} N_a^e N_b^e - \nabla N_a^e \cdot \frac{\partial \boldsymbol{q}}{\partial \phi} N_b^e \right. \\ \left. - \nabla N_a^e \cdot \left[\frac{\partial \boldsymbol{q}}{\partial \nabla\phi} \nabla N_b^e \right] - N_a^e N_b^e\, D\, f \right\} d\boldsymbol{x},\end{aligned} \tag{A.13}$$

where the sensitivity of the ionic flux is

$$D\, f = \frac{\mathrm{d} f(\phi, r^*(\phi))}{\mathrm{d}\phi} = \left\{ \frac{\partial f}{\partial \phi} + \frac{\partial f}{\partial r} \frac{\mathrm{d} r^*}{\mathrm{d}\phi} \right\} \Big|_{\phi^h, r^*}, \tag{A.14}$$

which in the particular case of the Aliev-Panfilov model takes the form

$$D\,f = c\,[\,-3\,\phi^2 + 2\,[1+\alpha]\,\phi - \alpha\,] - r - \phi\,\frac{\mathrm{d}r^*}{\mathrm{d}\phi}\,. \tag{A.15}$$

For the porous-medium diffusion law (2.5) we finally have

$$\frac{\partial \boldsymbol{q}}{\partial \phi} = -m\phi^{m-1}\boldsymbol{D}\nabla\phi \tag{A.16}$$

$$\frac{\partial \boldsymbol{q}}{\partial \nabla\phi} = -\phi^{m}\boldsymbol{D} \tag{A.17}$$

Denoting by $\Phi = [\phi_1, \ldots, \phi_{\mathrm{n_{nd}}}]$ the vector of the nodal potentials, for each iteration of the Newton-Raphson scheme we have the update

$$\Phi \leftarrow \Phi - \left\{ D\mathsf{R}^{\phi} \right\}^{-1} \mathsf{R}^{\phi} \tag{A.18}$$

which is performed until a convergence criteria is met, tipically based on the L^2 norm of R^{ϕ}.